If Baryon Asymmetry of the Universe (multiverse?) is due to CP violation

6×10^{-28} e-cm $< dn < 2 \times 10^{-25}$ e-cm

BUT

Standard Model (without theta problem)
10^{-33} e-cm $< dn < 10^{-31}$ e-cm

Theta problem: edm is very large prop to unkown parameter 'theta' which must be set to $\sim 10^{(-10)}$.
To avoid this Axions were invented => small industry of Axion searches

Edm searches are the best way to look for physics beyound the standard model because the expected standard model background is so small

1950 Purcell and Ramsey notice lack of experimental evidence for Parity conservation. Dirac monopole cited as a posssible source of P violation. Perform experimental search for neuron edm

1956 Lee and Yang suggest Parity is not conserved. At the time the nedm result was best experimental limit on P violation

1957 Smith, Purcell and Ramsey publish their experimental limit for the neutron edm.
Landau points out that a non-zero particle edm would violate T (CP) as well as P.
Madame Wu reports the direct observation of P violation

1958 Ramsey states that T violation is also an experimental question

1964 Discovery of CP violation in Ko decay

TABLE I: Some experimental limits on EDMs.

Physical System	Value, Error ($e \cdot$ cm)	Reference
^{199}Hg atom	$(-1.06 \pm 0.49 \pm 0.40) \times 10^{-28}$	[3]
electron	$(0.69 \pm 0.74) \times 10^{-27}$	[4]
neutron	$(-1.0 \pm 3.6) \times 10^{-26}$	[5]
muon	$(3.7 \pm 3.4) \times 10^{-19}$	[6]

Comparison of electric dipole moments and the Large Hadron Collider for probing CP violation in triple boson vertices

Sunghoon Jung[a], James D. Wells[b,a]

[a]*Michigan Center for Theoretical Physics (MCTP)*
University of Michigan, Ann Arbor, MI 48109-1120, USA

[b]*CERN, Theory Division, CH-1211 Geneva 23, Switzerland*
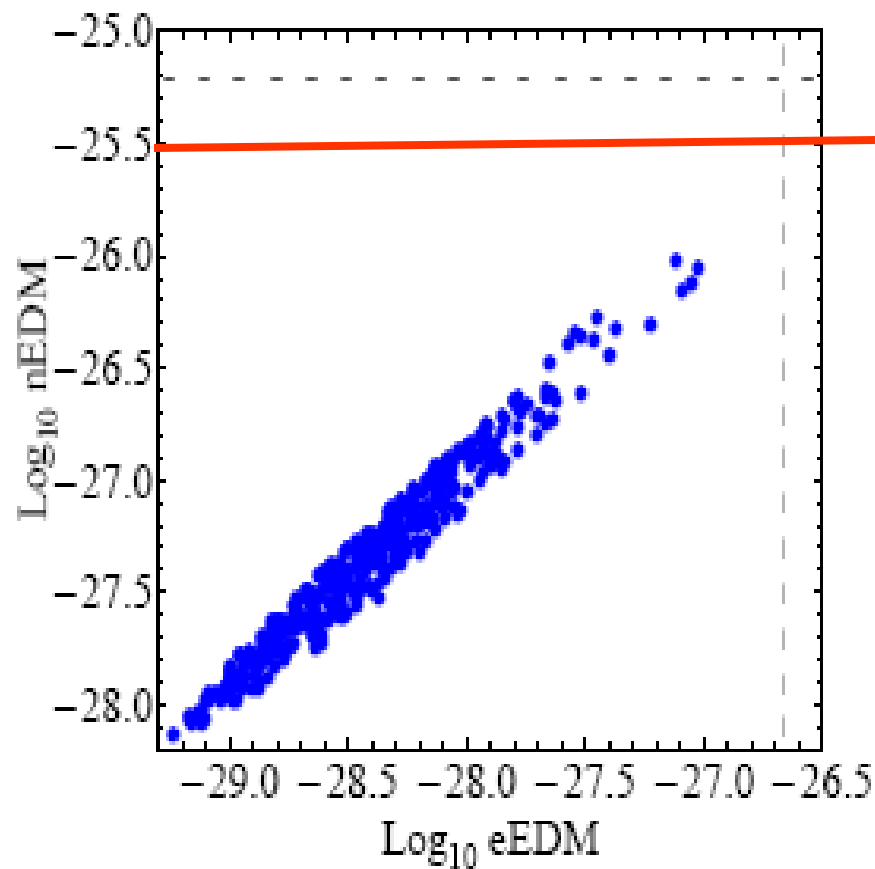
Figure 6: Scatter plot of electron EDM and neutron EDM in split supersymmetry. Input parameters are scattered within the range Eq.(2). Dashed lines represent the current experimental sensitivities.

An EDM Violates P and T

Magnetic dipole $= -\vec{\mu} \cdot \vec{B} = -\mu\vec{\sigma} \cdot \vec{B}$ $H_{Electric\ dipole} = -\vec{d} \cdot \vec{E} = -d\vec{\sigma} \cdot \vec{E}$
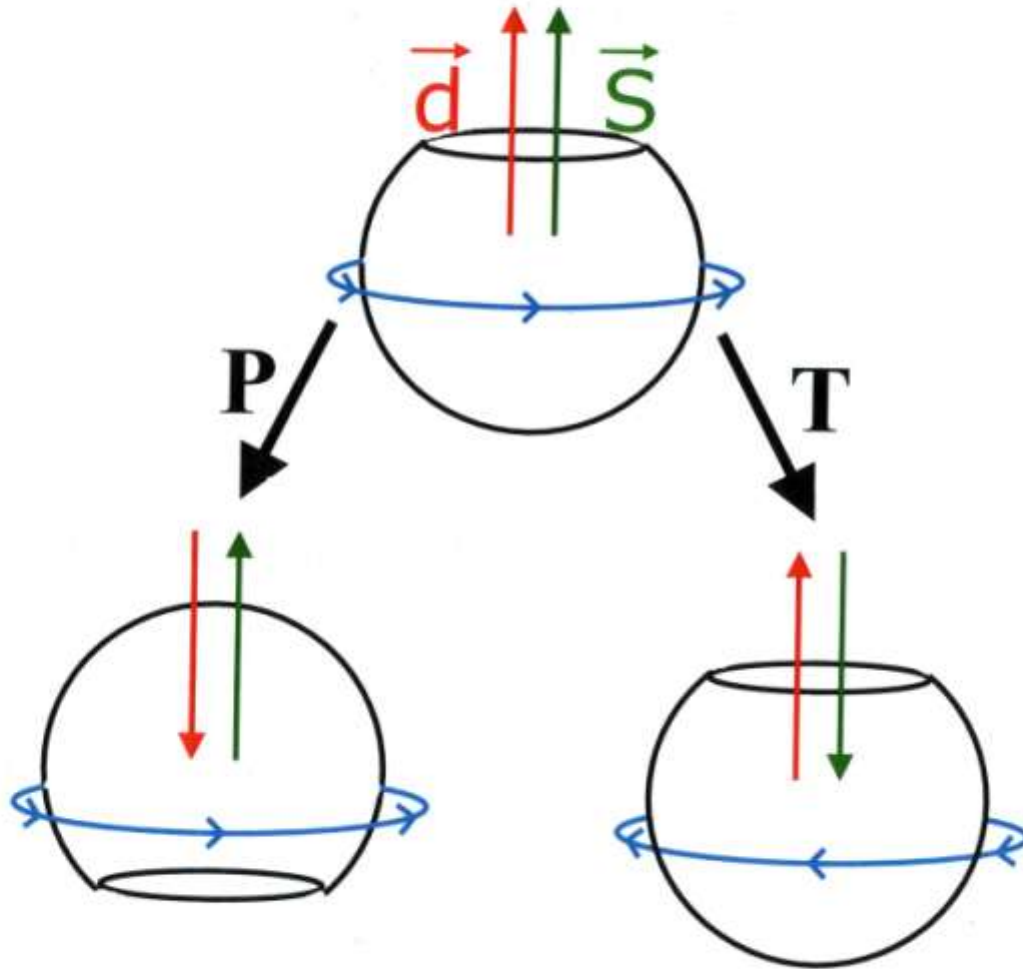
$$CPT\ theorem \Rightarrow T\text{-violation} = CP\text{-violation}$$
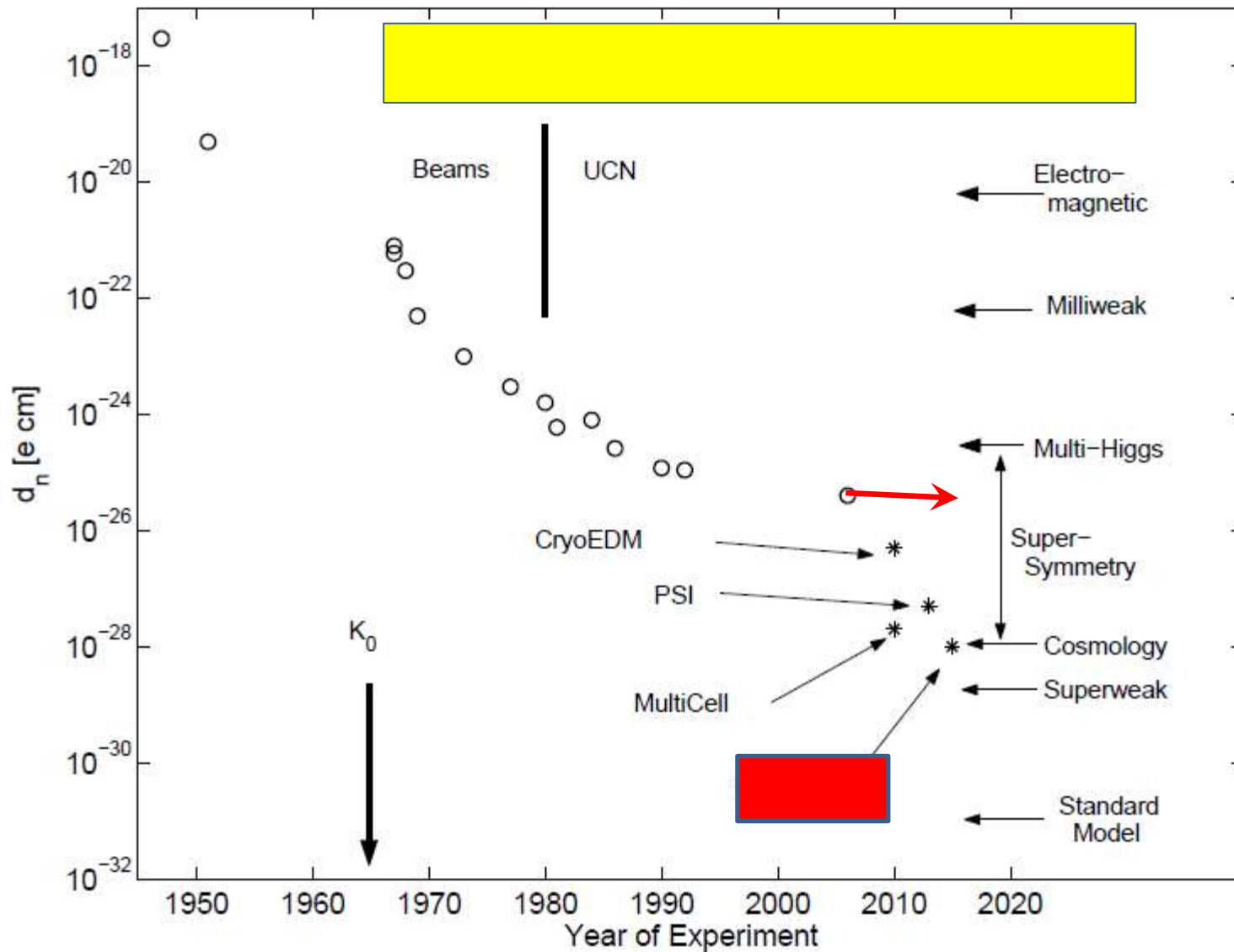
Fig. 1. Historical development of the neutron EDM experimental limit along with expectations from various theoretical models. The points marked with * are experiments presently under development or proposed, and will be discussed in this review.

Table 3. Comparison of neutron EDM experimental sensitivities, where the systematic limit represents the control required to attain the full fundamental shot noise sensitivity.

Technique	E [kV/cm]	T [s]	I [n/s]	Sys. Lim.	$ET\sqrt{I}$
Bragg reflection	1×10^9	2×10^{-7}	10^4	$\theta_{EB} < 10^{-4}$	2×10^4
Pendellösung (α-quartz)	2×10^8	2×10^{-3}	2×10^3	$\theta_{EB} < 10^{-7}$	2×10^7

$$\vec{B}_m = \frac{\vec{v}}{c} \times \vec{E}. \tag{8}$$

For a typical cold neutron velocity of $v = 1000$ m/s in an electric field of 100 kV/cm, $B_m = 1$ mG. Now consider an experiment where there is a large applied magnetic field $\vec{B}_0$ and an EDM is sought by measuring the shift in Larmor precession frequency on reversal of a electric field $\vec{E}$, as implied by (6).
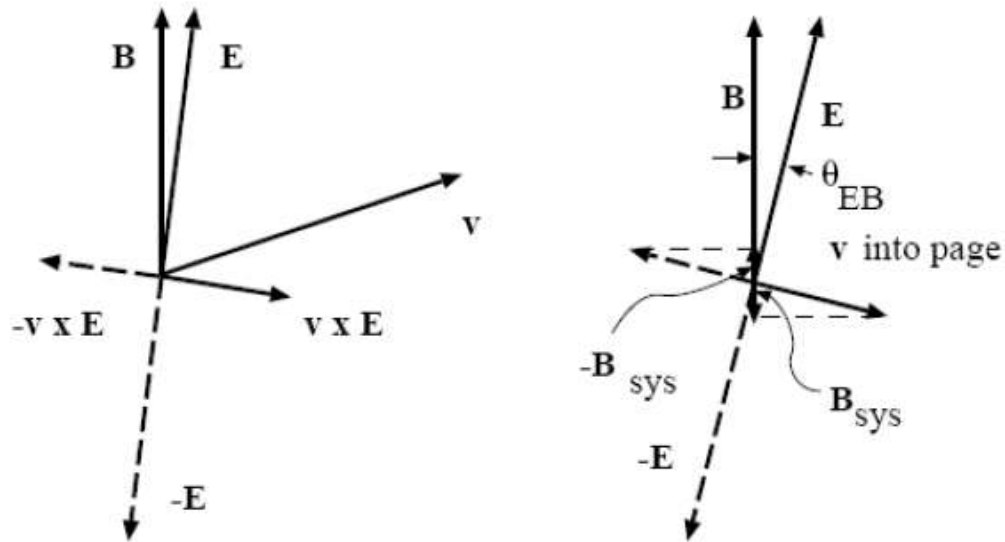
Fig. 2.   . Geometrical picture of the $\vec{v} \times \vec{E}$ effective magnetic field.

If $\vec{E}$ and $\vec{B}_0$ are nearly parallel as shown in Fig. 2, and $B_m \ll B$, the effective magnetic field strength is given by the magnitude of $\vec{B} = \vec{B}_0 + \vec{B}_m$

$$B = B_0 + \theta_{EB} B_m + \frac{1}{2} \frac{B_m^2}{B_0}, \tag{9}$$

Beam experiments became less attractive because of
E x V and increased sensitivity of UCN

Beginning of a series of room temperature UCN experiments

Ultra-Cold Neutrons (UCN)

- E<Vc   critical energy for total refelction
- UCN totally reflected for all angles of incidence

$$E \sim 10^2 \, nev$$ $$\lambda \sim 500 \, \overset{o}{A}$$ T~1mK h~1m (mgh~E)

B~2 Tesla (uB~E)

V
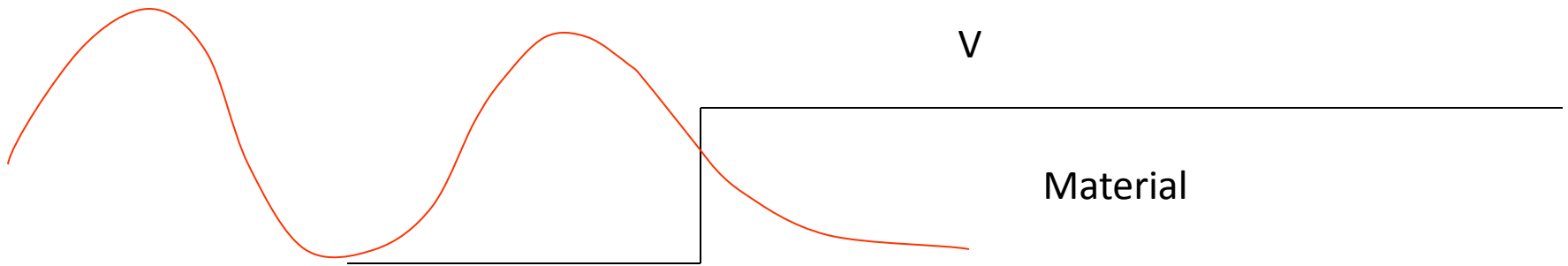
Material

Wave fn penetrates material -> wall losses limit storage time

Leningrad 1986, UCN experiment
Two chambers, plagued by leakage currents,
field fluctuations
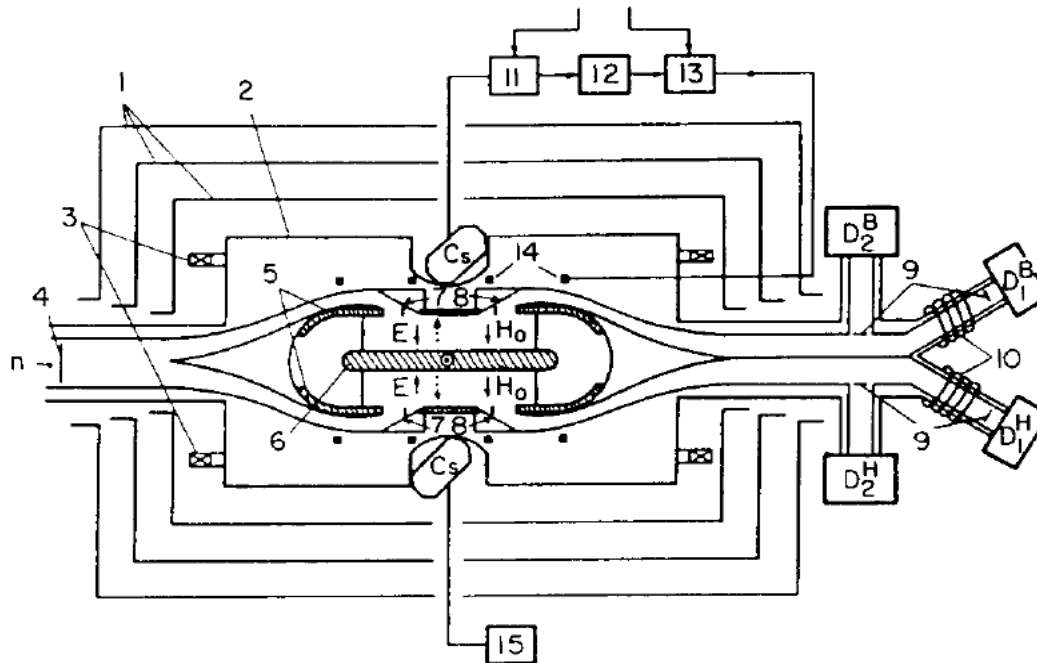
Figure 7.17 The neutron EDM apparatus used at the Leningrad reactor: 1, magnetic shields; 2, vacuum chamber; 3, Helmholtz coils for producing the static magnetic field; 4, UCN polarizer; 5, ground electrodes; 6, high voltage electrode; 7, entrance shutters; 8, exit shutters; 9, analysers; 10, spin flippers; 11, caesium magnetometers; 12, frequency divider; 13, control for oscillating field pulses; 14, coils for producing oscillating field; 15, caesium magnetometer; D labels the UCN detectors with B and H specifying upper and lower chambers, 1 and 2 specifies the two polarizations (Altarev *et al* 1986b).

Sussex, RAL, ILL experiment
Single cell, co-magnetometer.
Plagued by field fluctuations and geometrice phase
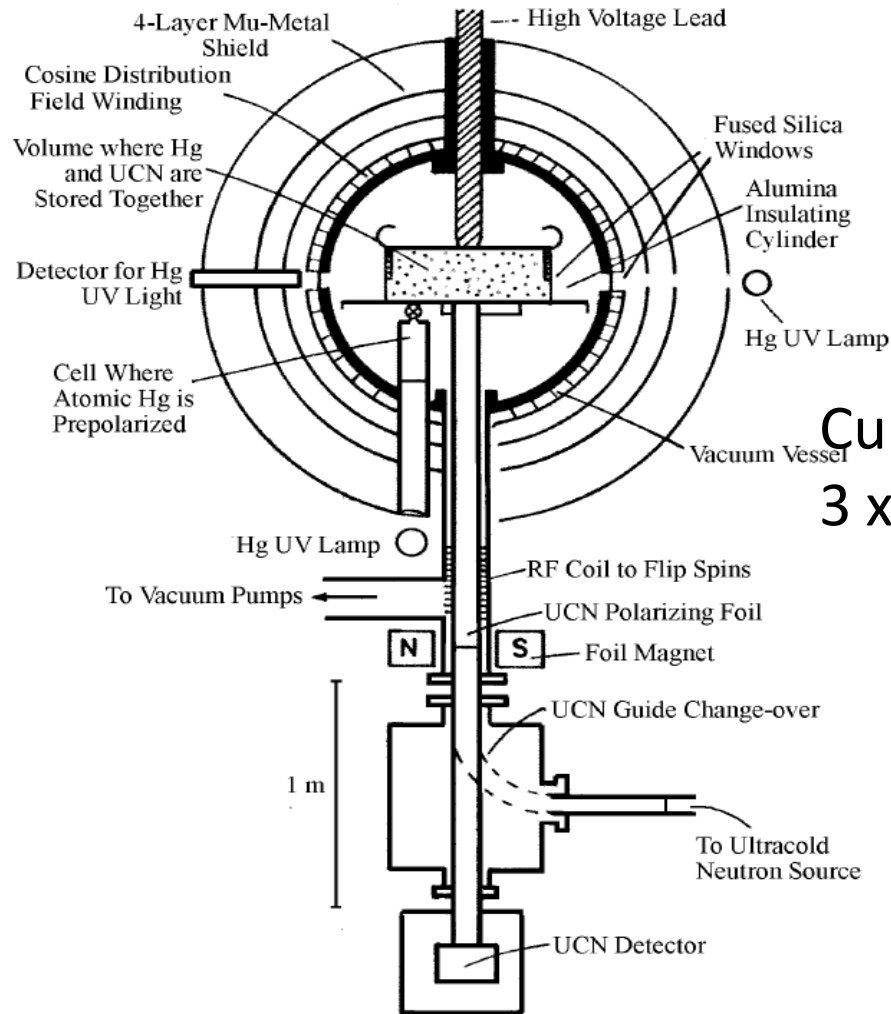
Current best value..
3 x 10^(-26) e-cm

Fig. 9.   Schematic of the ILL UCN EDM experiment incorporating a ^{199}Hg comagnetometer

Need for a co-magnetometer
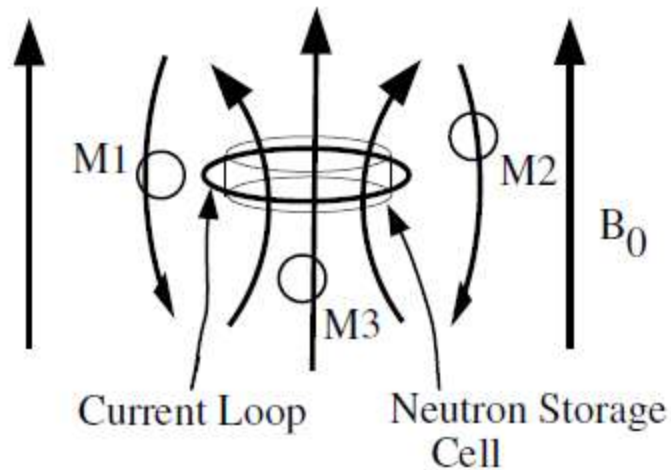
Fig. 3. The external magnetometer problem. Leakage currents associated with the application of a high voltage to the measurement cell can flow in a loop (or some fraction thereof) around the cell, creating a magnetic field that is correlated with the direction of the electric field. Depending on the location of a magnetometer, the field from the loop can add or subtract to the applied static field B_0.

Based on these results we decided to go for a
Superconducting shield (cryogenic experiment)
And a co-magnetometer

Current projects

- **Active worldwide effort to improve neutron EDM sensitivity**

Exp	UCN source	cell	Measurement techniques
	Superfluid ^{4}He Superconducting Shield	^{4}He	Ramsey technique for ω External SQUID magnetometers No co-magnetometer
PNPI – I LL	ILL turbine PNPI/Solid D_2	Vac.	Ramsey technique for ω E=0 cell for magnetometer
ILL Crystal	Cold n Beam		Crystal Diffraction
	Solid D_2	Vac.	Ramsey technique for ω External Cs & ^{3}He magnetometers Hg co-mag for P1, Xe for P2?
	Superfluid ^{4}He Superconducting Shield	^{4}He	^{3}He capture for ω ^{3}He comagnetometer SQUIDS & Dressed spins
TRIUMF/JPARC	Superfluid ^{4}He Superconducting Shield?	Vac.	Under Development

Comparison of Capabilities

	CRYO EDM1	CRYO EDM2	PSI EDM1	PSI EDM2	SNS EDM
$\Delta\omega$ via accumulated phase in n polarization	🟩	🟩	🟩	🟩	🟥
$\Delta\omega$ via light oscillation in ^{3}He capture	🟥	🟥	🟥	🟥	🟩
Co-magnetometer	🟥	🟥	🟩	?	🟩
Superconducting B-shield	🟩	🟩	🟥	🟥	🟩
Dressed Spin Technique	🟥	🟥	🟩	🟩	🟩
Horizontal B-field	🟩	🟩	🟥	🟥	🟩
Multiple EDM cells	🟥	🟩	🟥	🟩	🟩

Note that red vs green does not necessarily signify good vs bad
But understanding systematics requires mix of red & green

🟩 = included

🟥 = not included

What IF?

The Sussex-ILL experiment had no co-magnetometer

Non-zero edm,

Great sensation

Dozens of wrong theories calculating their number

Munich, most comprehensive attempt at a room temperature experiment..Temp controlled high efficiency shields, complex field stabilization
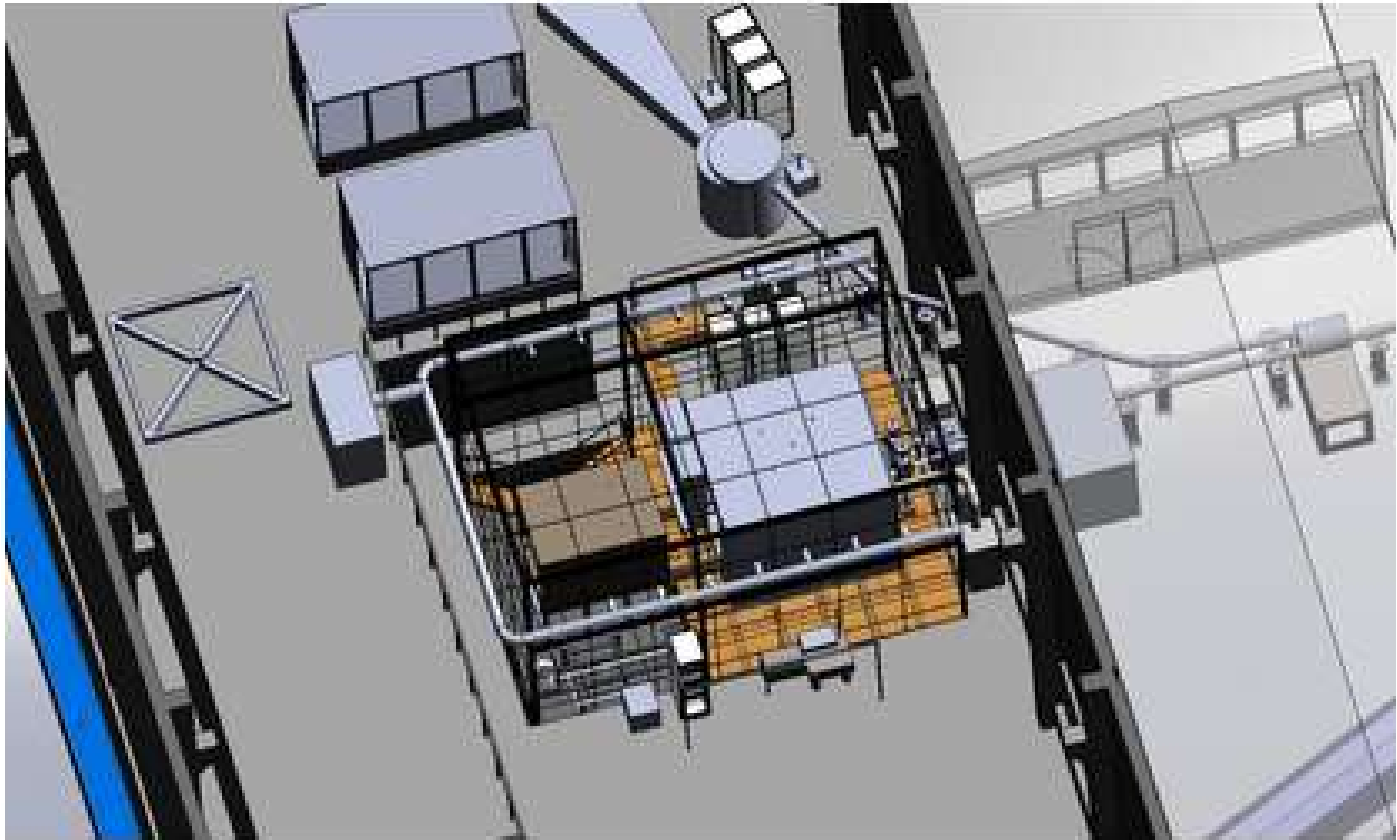
What is Unique About Our Experiment

- **Production of ultracold neutrons (UCN) within the apparatus**
  - *higher UCN density and longer storage times*

- **Use of liquid as a high voltage insulator**
  - *higher electric fields*

- **Use of a ^{3}He co-magnetometer and superconducting shield**
  - *better control of magnetic field systematics*

- **Employ two different measurement techniques**
  - *oscillation of scintillation rate and dressed spin techniques*

Tackling unknown systematic effects requires unique handles in the experiment that can be varied.

Polarized He3 as:

-Polarizer (partial..beam is polarized
-Magnetometer
-Analyzer
-Detector

Dilution refrigerator

He3 polarizer
Stern Gerlach

He3 injection volume

Magnetic shield
house

High voltage amplifier

NEUTRON
BEAM

Measuuurement cells
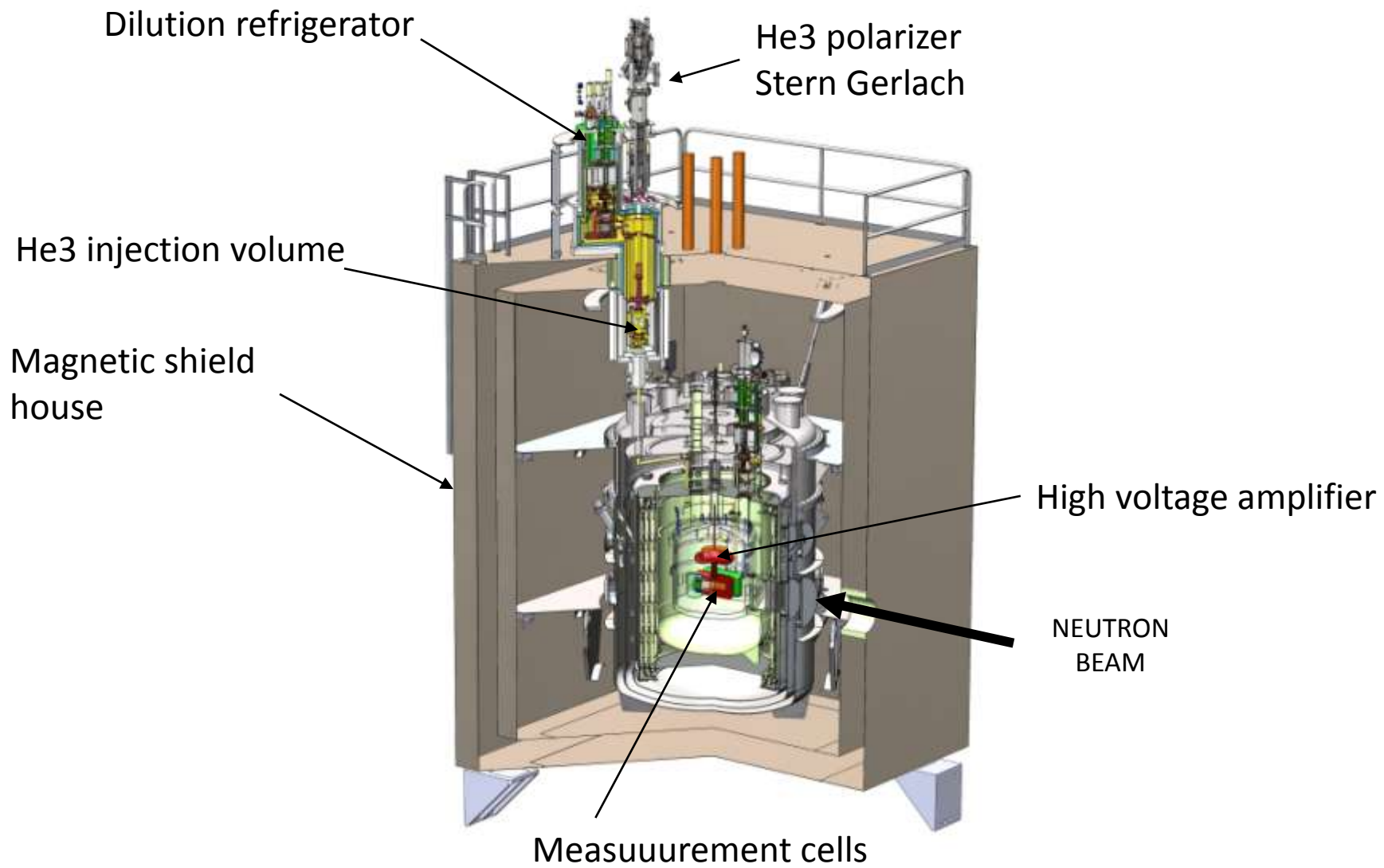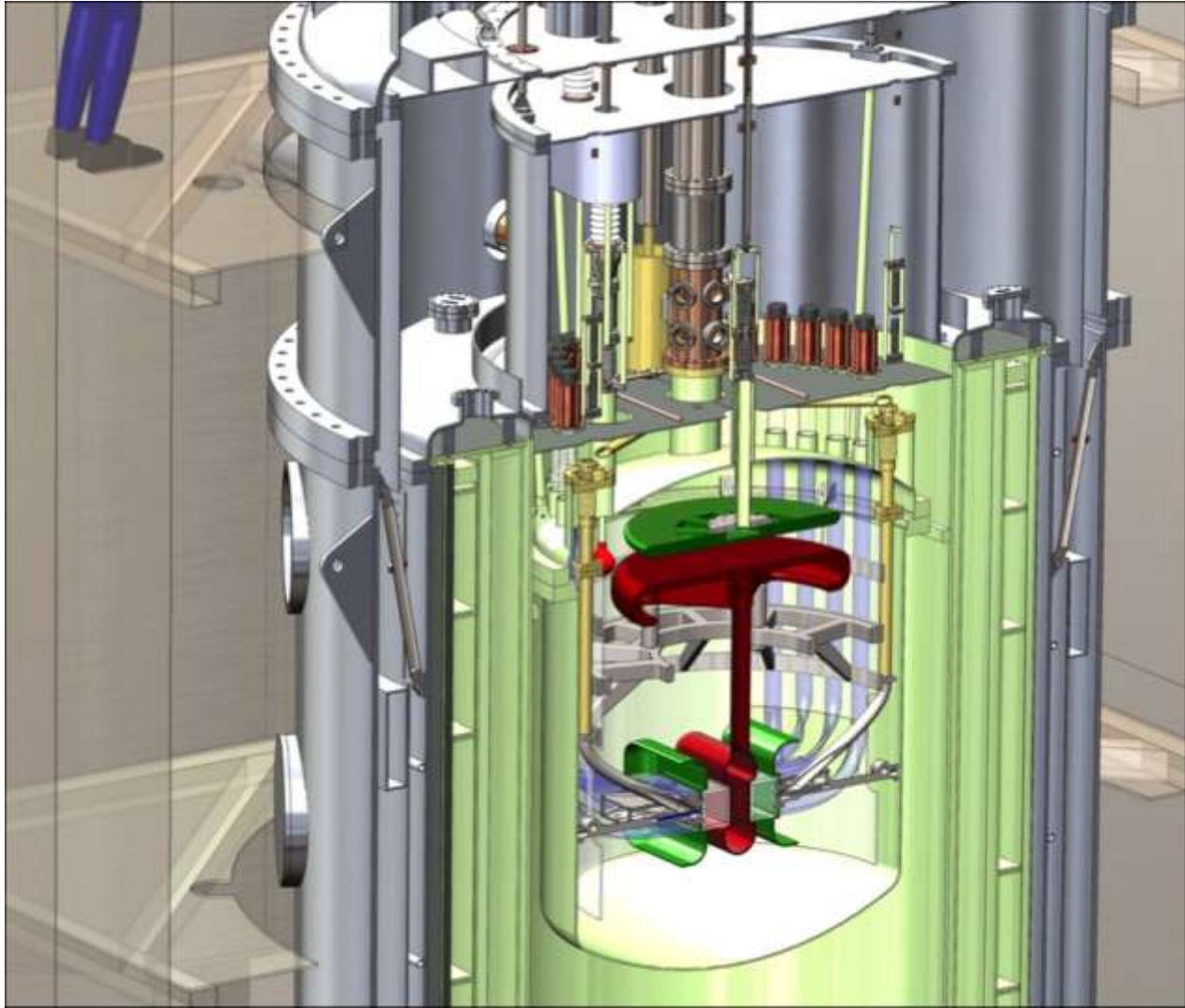
Key Experimental Concepts

- Ultracold Neutrons/Superthermal Production

- ^{3}He Co-Magnetometry

- Charge Particle Detection in Liquid Helium

Superthermal Production of UCN

- 8.9 Å (12 K or 0.95 meV) neutrons can scatter in liquid helium to near rest by emission of a single phonon.
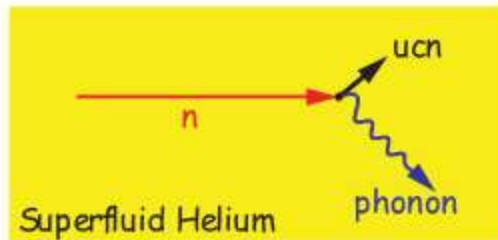
Golub and Pendlebury

Superfluid Helium
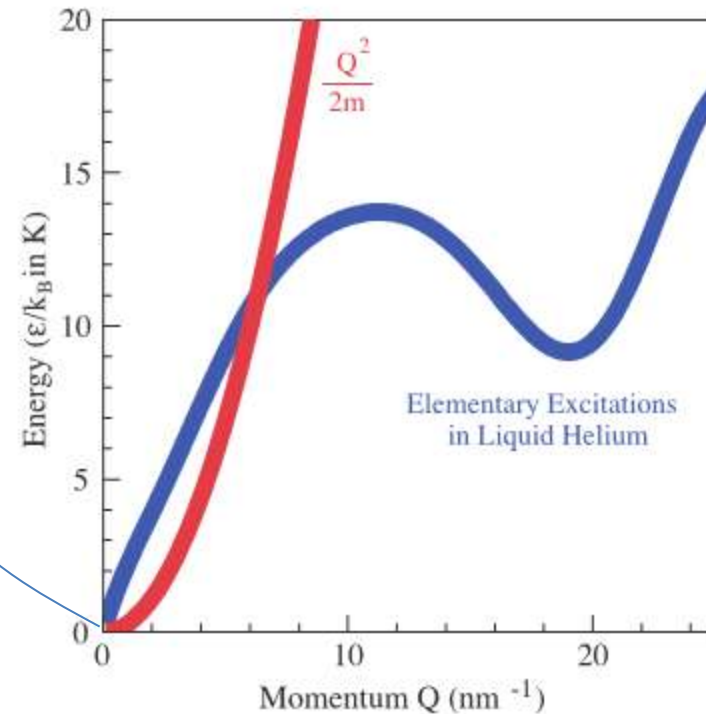
- Upscattering (by 12 K phonon absorption)

  ~ Population of 12 K phonons
  ~ $e^{-12\,K/T_{bath}}$

Co-Magnetometry

Neutron

^{3}He

B E

B E
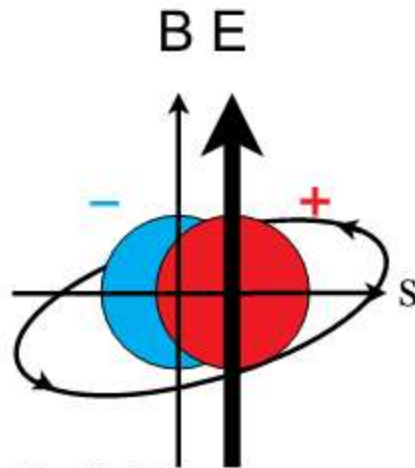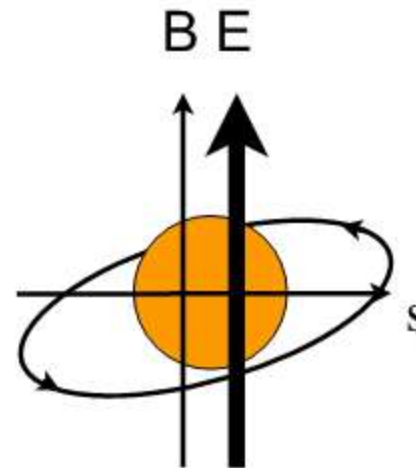
$f_3 = \gamma_3 B$

$\gamma_3 = 1.1\ \gamma_n$

$f_n = \gamma_n B \pm 2\ d_n E$

- Look for a difference in precession frequency
  $f_n - f_3 = (\gamma_n - \gamma_3)\ B \pm 2\ d_n E = (0.1\ \gamma_n)\ B \pm 2\ d_n E$

- Detect precession of ^{3}He magnetization by SQUIDS which serves as a direct magnetometer ($d_{3He} << d_n$)

Collaborating Institutions

- **Hahn-Meitner Institut, Berlin**
- **NIST/Gaithersburg**
- **Harvard**
- **Simon Fraser University**
- **Caltech**
- **University of Illinois**
- **Los Alamos National Laboratory**
- **Berkeley**
- **Duke**
- **Oak Ridge National Laboratory**
- **University of Leiden**
- **University of New Mexico**
- **North Carolina State University**

Boston U
MIT
Yale
Old Miss

Physics

Los Alamos

Neutrons inside the superfluid helium can be detected via the energetic charged particles which are produced in the beta decay:

$$n \longrightarrow p + e^- + \bar{\nu} + 783 \text{ keV}$$
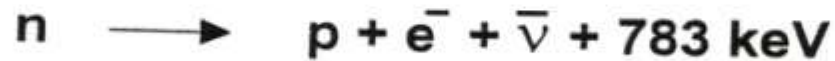
or with a dilute solution of ^{3}He inside the ^{4}He volume:

$$n + {}^3\text{He} \longrightarrow p + {}^3\text{H} + 764 \text{ keV}$$
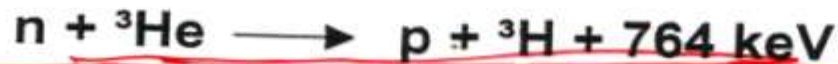
Travelling through the helium these charged particles loose their kinetic energy which is partially converted into scintillation light.

$\longrightarrow$ Scintillations with highest intensity in vacuum ultraviolet region (VUV) of the optical spectrum.

Using a fluorescent wavelength shifter the VUV scintillation light is converted into visible light which can easily be detected by a photomultiplier.

liquid helium

He$_2$*

$\gamma - 430$nm

e$^-$

$\gamma - 80$nm

TPB

TPB Doped Polystyrene

Clear Acrylic

Neutron Shielding

Thermal Link to Mixing Chamber

250 mK

4 K

77-300 K

liquid helium

He$_2$*

$\gamma \sim 430$nm

e$^-$

$\gamma \sim 80$nm

TPB

5 cm

40 cm

60 cm

Teflon Window

Neutron Collimator

Cupronickel Tube

Beam Dump

Ultra-pure Helium Fill Line
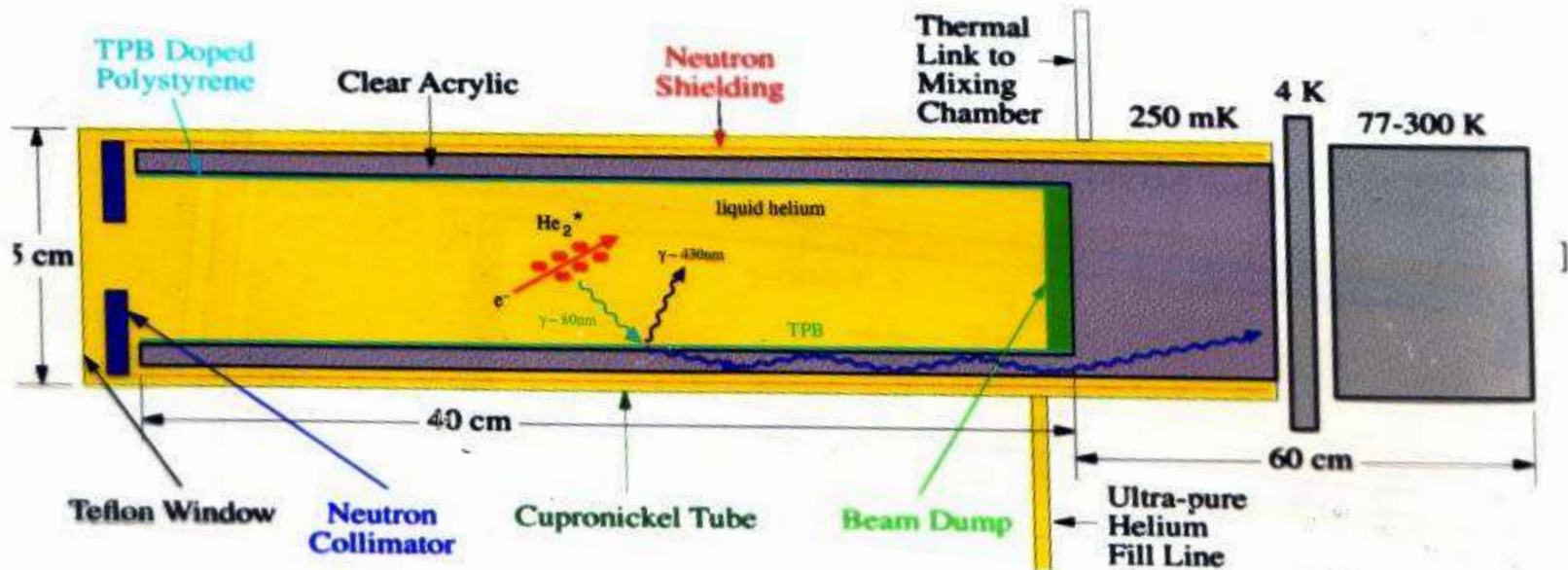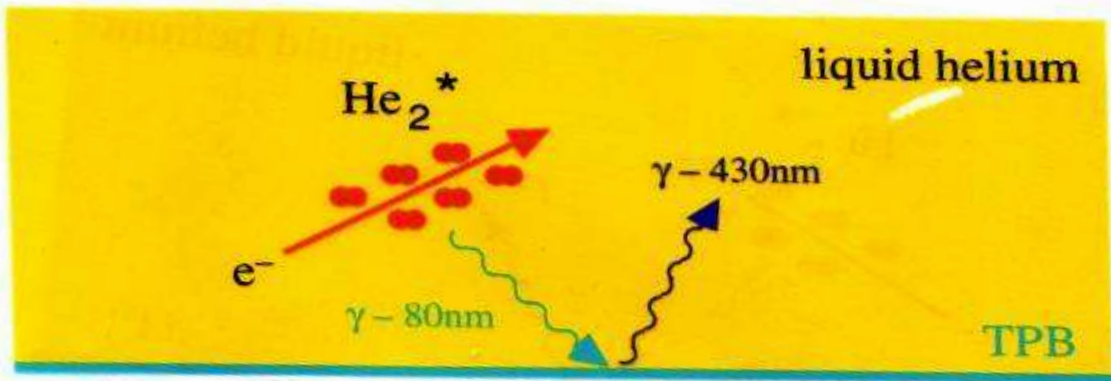
Neutron absorption by He3

experimentally
$$\frac{\sigma_{J=0}}{\sigma_{tot}} = 1.01 \pm .03$$

$$\vec{I} \parallel \vec{S} \Rightarrow \sigma_{He3} = 0$$

$$\frac{1}{\tau_{\pm}} = \frac{1}{\tau_{\beta}} + (1 \overset{\textcolor{red}{+/-}}{\mp} \qquad) v_n$$

Scintillation Rate

$$= \frac{\rho_{UCN}}{\tau_{abs}} \approx \left(1 - \vec{P}_n \cdot \vec{P}_3 \right) = \left(1 - P_n P_3 \cos\theta_{n3}(t) \right)$$
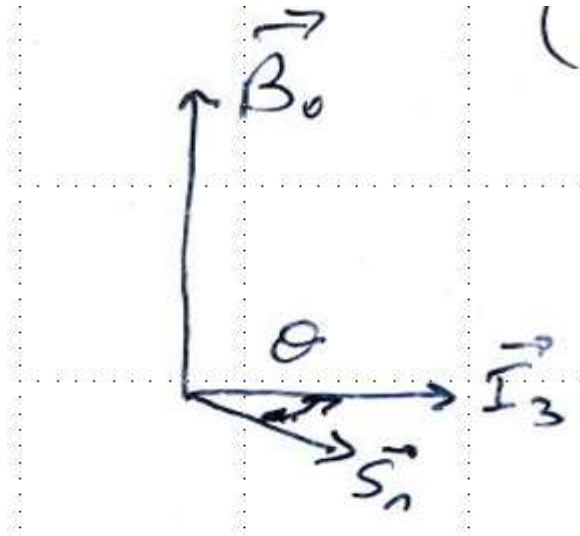
$$\theta = (\gamma_n - \gamma_3) B_o t \pm \frac{ed_n}{\hbar} t$$

$$\gamma_3 = 1.1\gamma_n$$

Factor of 10 reduction in Field sensitivity

$$\omega_{eff} = .1\gamma_n B_o$$

Dressed Neutron
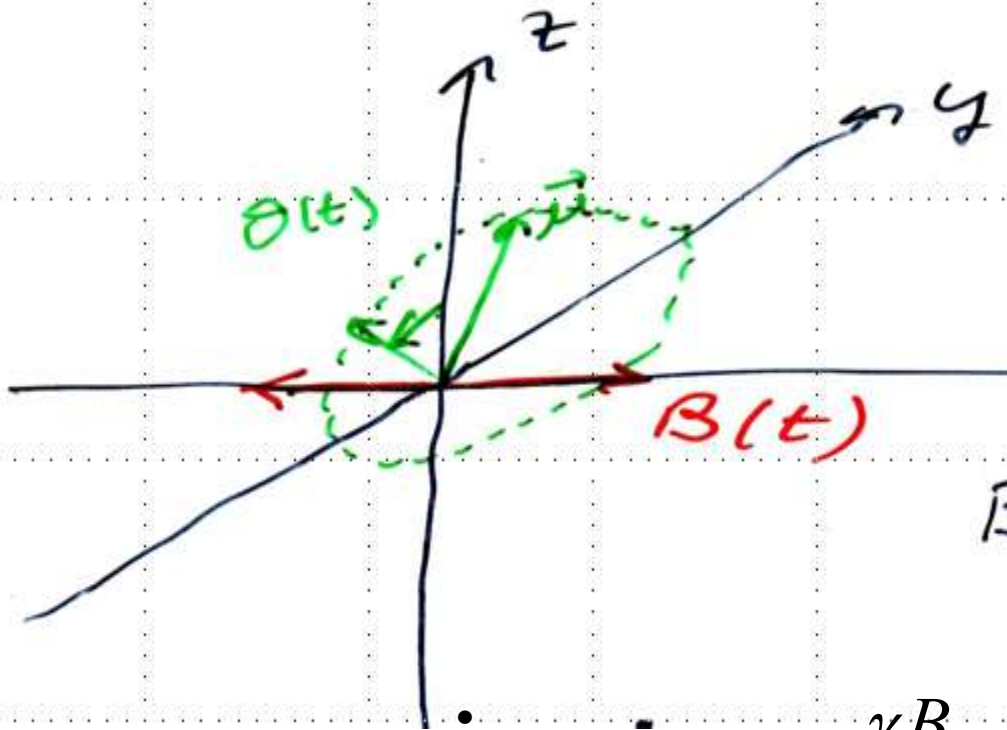
$$B(t) = B_d \sin \omega_d t$$

$$\omega_{prec} = \gamma B(t) = \dot{\theta}(t) \qquad \theta = \frac{\gamma B_d}{\omega_d} \cos \omega_d t$$

$$\langle \cos \theta \rangle = \frac{1}{T} \int dt \cos\left[\frac{\gamma B_d}{\omega_d} \cos \omega_d t \right] = J_o\left(\frac{\gamma B_d}{\omega_d} \right) = J_o(x) = \gamma_{eff}$$

$$\text{X=dressing parameter} \quad = \left(\frac{\gamma B_d}{\omega_d} \right)$$

Critical dressing.

- The gyromagnetic ratio's can effectively be made equal by applying a RF field to achieve critical dressing.

$$\langle \cos(\theta) \rangle_T = \frac{1}{T} \int_T dt \cos\left[\left(\frac{\gamma B_{rf}}{\omega_{rf}}\right) \cos(\omega_{rf} t)\right] = J_0\left(\frac{\gamma B_{rf}}{\omega_{rf}}\right)$$

- To solve for the critical dressing set

$$\gamma_n J_0(x_n) - \gamma_3 J_0(x_3) = 0,$$

$$x_i = \gamma_i B_{rf}/\omega_{rf}$$

$$x_c \approx 1.19, \quad J_0(x_c) = 0.65.$$

Principle of Dressed Spin

$$\gamma' = \gamma J_o (\gamma B_{rf} / \omega_{rf})$$

$$\gamma_3 = 1.1 \gamma_n$$

$$\gamma_n' = \gamma_3' \qquad \text{when} \qquad \gamma_n B_{rf} / \omega_{rf} \approx 1.1$$

We want $B_{rf} \gg B_0$ (1-10 mG) so B_{rf} is around 1 G, $\omega_{rf}/2\pi$ near 3 kHz

RF field must be homogeneous at the 0.1-1% level

Heating and gradients due to eddy currents present design challenges

Eliminates need for SQUID magnetometers and might increase
the sensitivity of the experiment
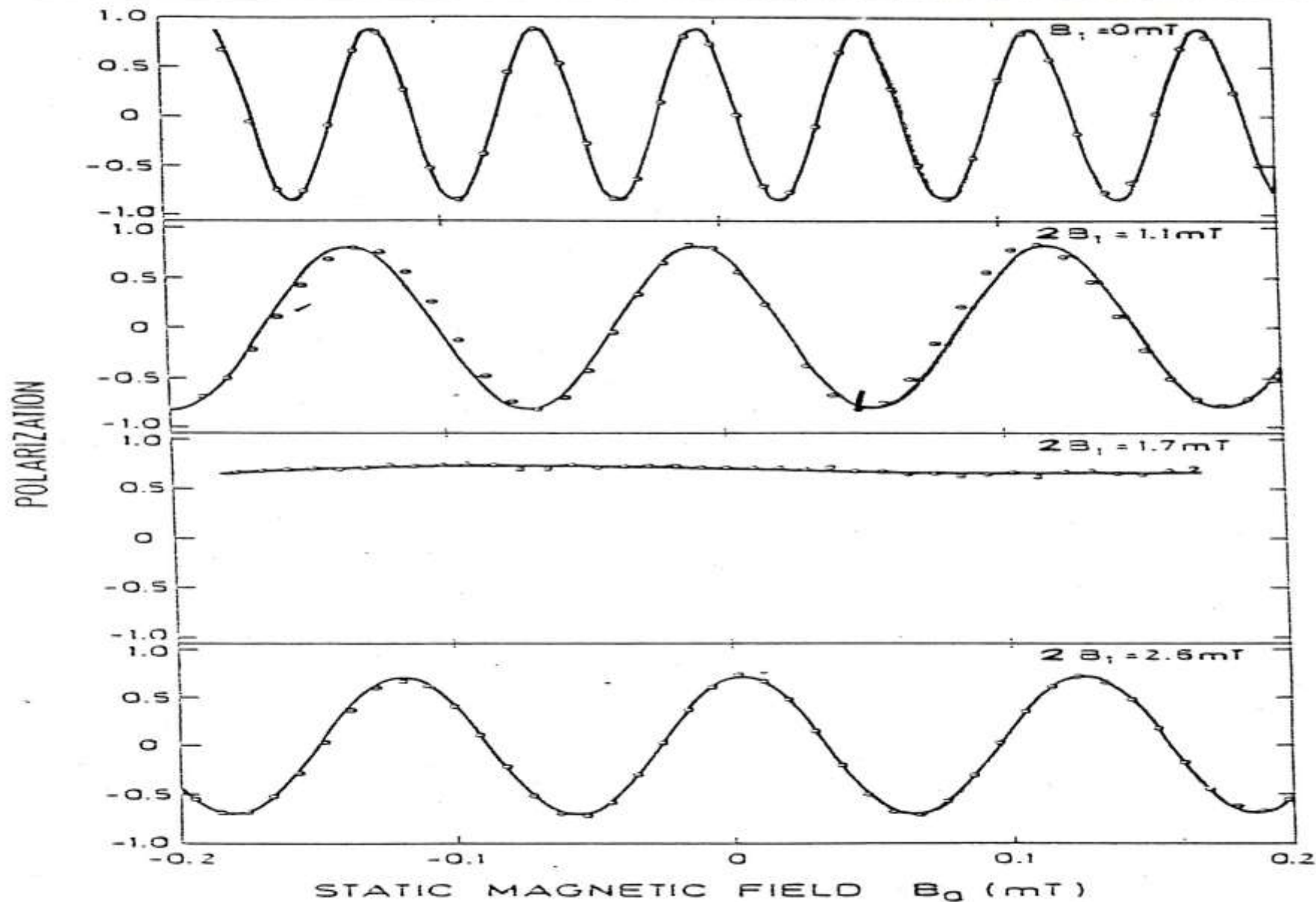
FIG. 3. Spin-precession measurements with dressed neutrons. At the critical rf-field strength $2B_1 = 1.7$ mT the g factor of the dressed neutron vanishes, and neutron spin-precession disappears.

CRITICAL DRESSING

$J_0(x)$
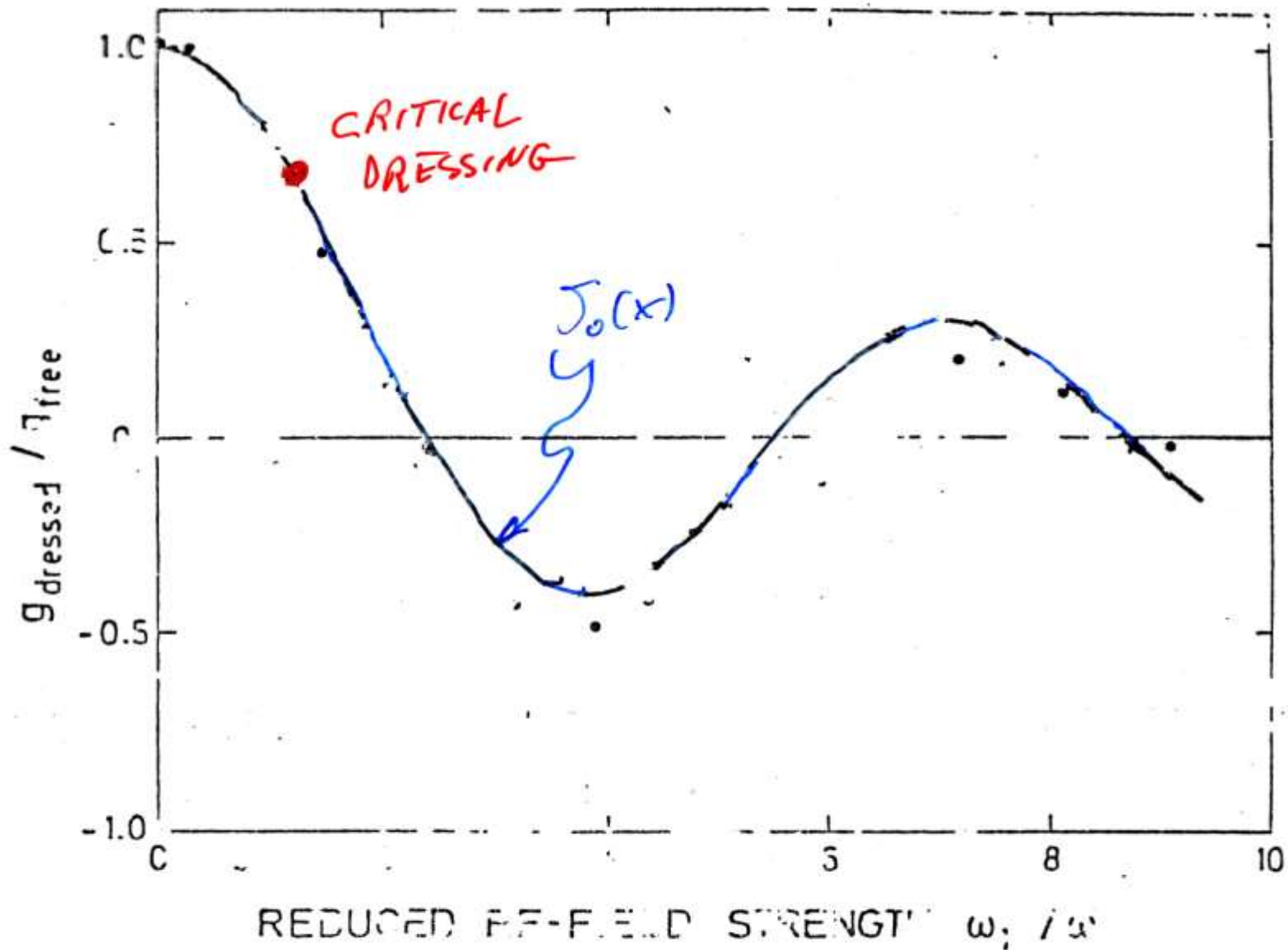
FIG. 4. Variation of the dressed-neutron's g factor with rf-field strength ($\omega_1 = \gamma B_1$).

Edm   apply electric field
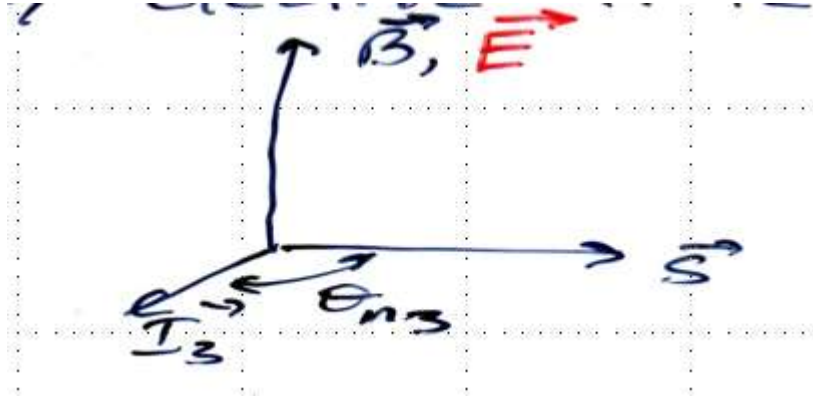
$$\omega_n = \gamma_{eff} B_o \pm \frac{e d_n E}{\hbar} . J\ (x)$$

$$\theta_{n3} = \frac{e d_n E}{\hbar} t$$ Shows up in scintillation rate

with $\vec{S}, \vec{I}$ parallel

Absortpion = 0

Modulate x

$$x(t) = x_{cr} + \varepsilon \cos \omega_m t$$

$$\gamma \omega_{n3} \approx \varepsilon \cos \omega_m t \pm kd_n E$$

$$\delta\theta \approx \qquad \pm kd_n E t$$

$$\left(\delta\theta_o \right)$$

Scintillation rate
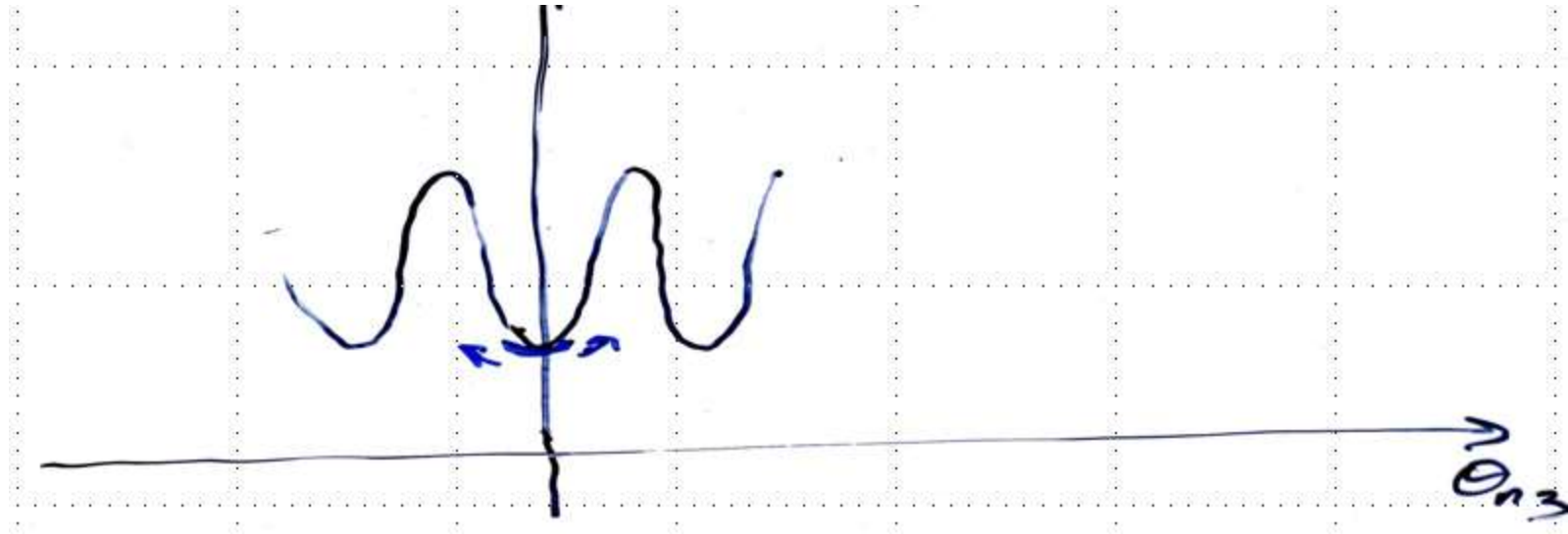
$$\frac{\partial S}{\partial \theta_{n3}} = 0 \Rightarrow \quad \text{Second harmonic} \quad \propto (\delta\theta)^2$$

$$\delta\theta = \delta\theta_o\left(\omega_m t\right) \pm kd_n Et$$

$$(\delta\theta)^2 \propto \pm\delta\theta_o\left(\omega_m t\right)kd_n Et$$

First harmonic growing
with time   →   edm!

Second harmonic for calibration

False nEDM effects measured at ILL

Hg

UCN

$+$

$-$

B_o

Δz

gradient coils
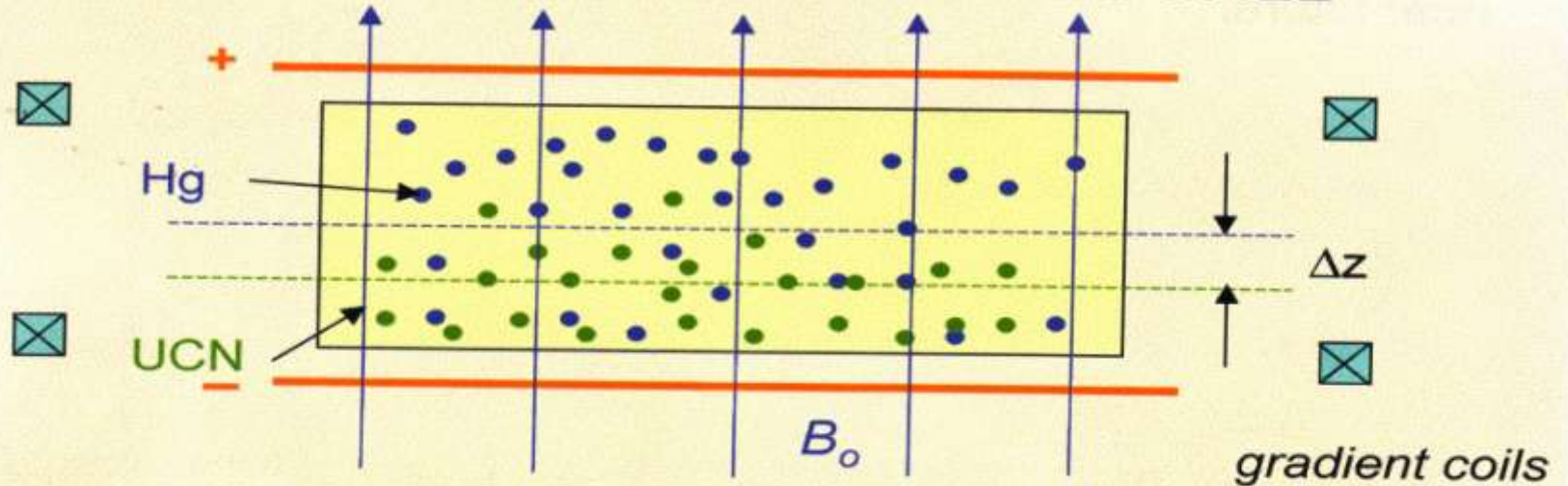
observed: $\omega_n / \omega_{Hg} \neq (\mu_n / \mu_{Hg})_{literature}$

Let $\partial B / \partial z \neq 0 : \quad \Delta B = \partial B / \partial z \cdot \Delta z$

Magnetic field

Perpendiculat to v

Rotates with v

$$\frac{\vec{v}}{c} \times \vec{E}$$
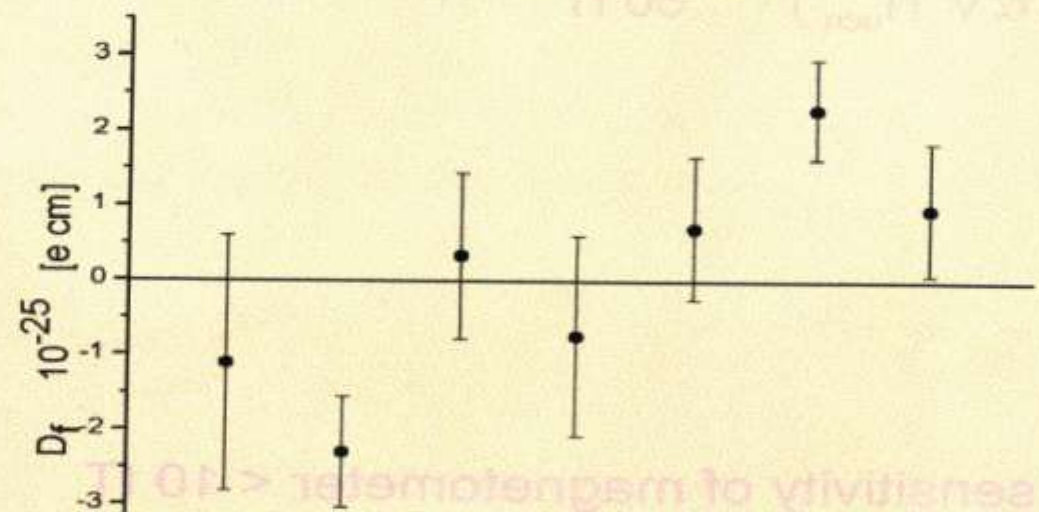
BLOCH-SIEGERT

Frequency shift ~ E^2

However   If $B_r \sim r$

then $\left(B_r + v \times E\right)^2 \propto E$

Important systematic effect $\delta\omega \sim \frac{\partial B_z}{\partial z} v$ E

Discovered by Cummins…molecular beam edm experiment
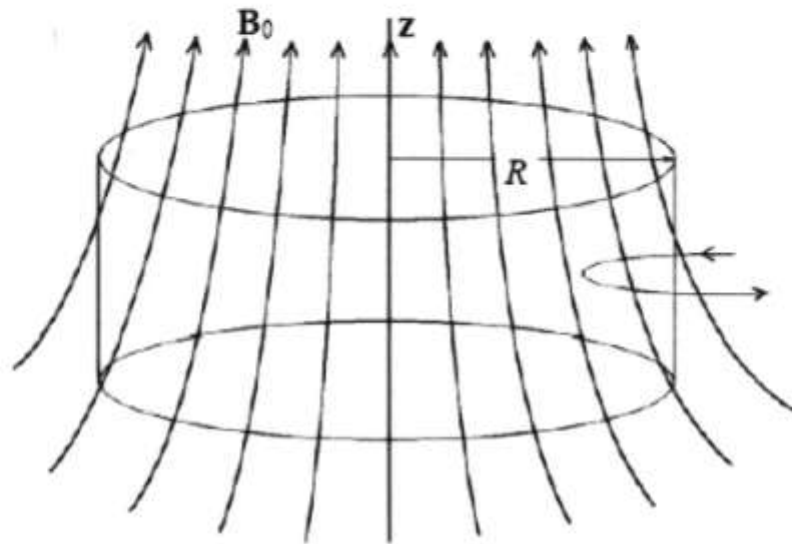
FIG. 1. Showing the shape of the B_0 field lines, when there is a positive gradient $\partial B_{0z}/\partial z$, shown in relation to an outline of the trap used to store ^{199}Hg atoms and UCN for the neutron EDM measurements at the ILL. If another field is superimposed having lines that both enter and leave through the sidewalls, like the one on the right hand side, it will be shown later that it does not affect the false EDM signals that are generated.

$$\vec{\nabla} \cdot \vec{B} = 0$$

$$B_r = \frac{1}{2} \frac{\partial B_z}{\partial z} r$$
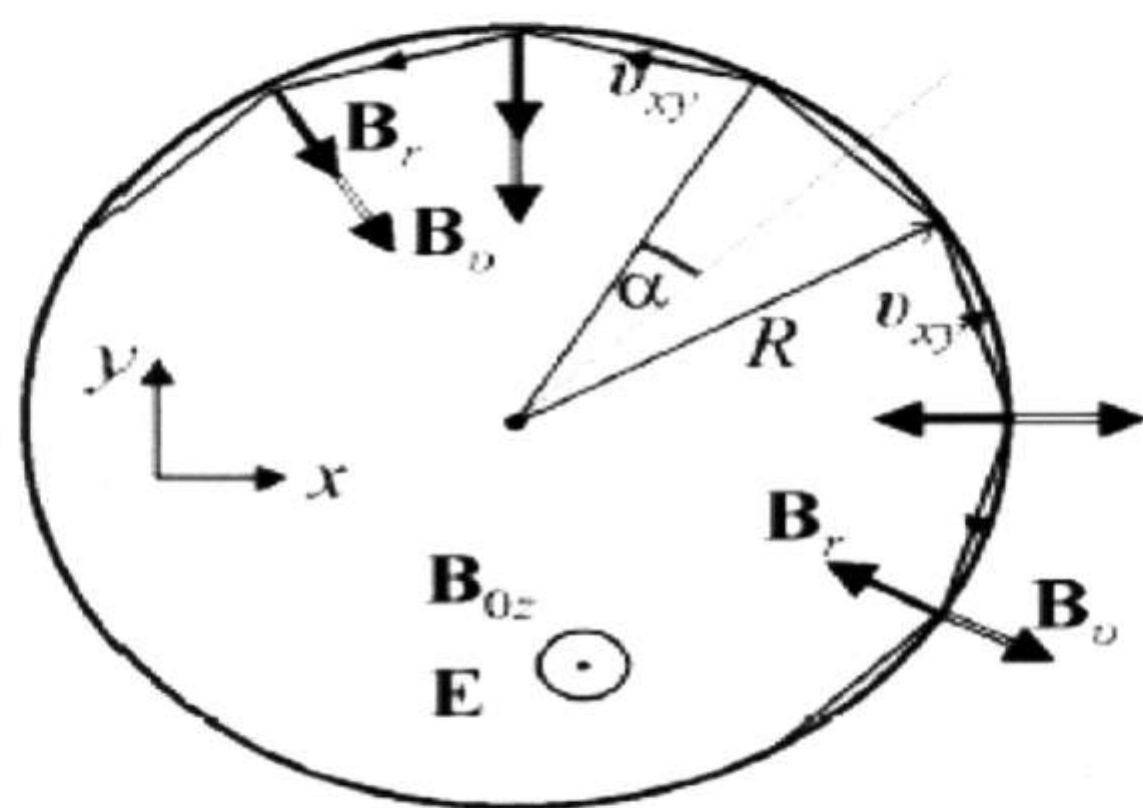
FIG 3. A view of the xy-plane of the trap bounded by the circular sidewall. Part of an orbit is shown projected onto the xy-plane for a particle undergoing specular reflection. The orbit is characterised by the angle α. Vectors E and B_{0z} point towards the reader and $\partial B_{0z}/\partial z$ is positive.

$$\tau_a = 2\frac{R\sin\alpha}{v}$$

$$W_r = \frac{2\alpha}{} = \alpha v$$

Bo, E

z

$\omega_o - \omega_r$

y

ω_r

$\omega_1 = \omega_{xy} \pm \omega_E$

x
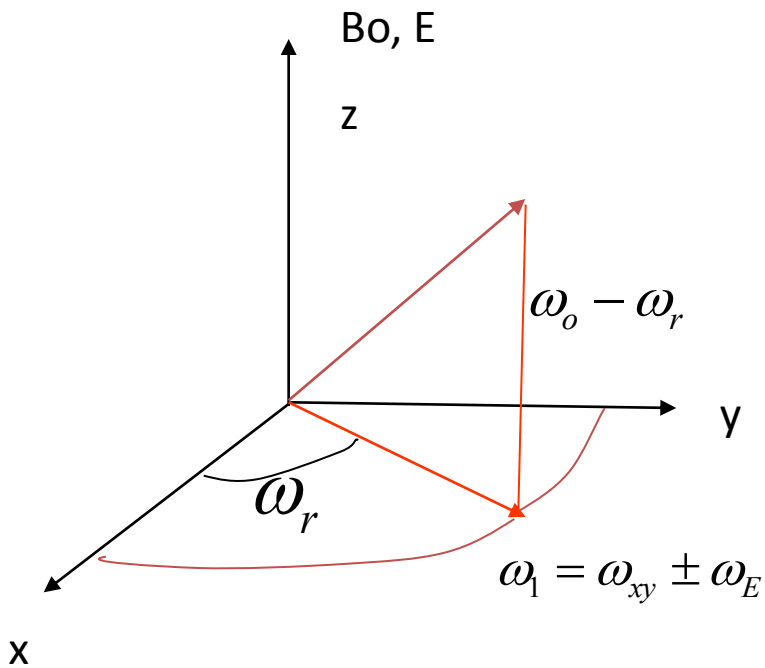
$$\omega_E = \gamma \frac{v}{c} E$$

$$\omega_{xy} = \frac{\partial B_z}{\partial z} \vec{r}$$

$$\omega_r = \frac{v}{r}$$

$$\omega - \omega_r = \left[(\omega_o - \omega_r)^2 + \omega_1^2 \right]^{1/2} \approx \omega_o - \omega_r + \frac{\omega_1^2}{2(\omega_o - \omega_r)}$$

Bloch-Siegert

Average over +/- v

$$\delta\omega \sim \frac{\omega_1^2}{2(\omega_o - \omega_r)} \Rightarrow \pm \frac{\omega_{xy} \frac{v}{c} E}{(\omega_o \mp \omega_r)}$$

N.F. Ramsey (PR 100 (1955) 1191) : $\omega \neq \omega_o$

$\Delta\omega_{BS}/\omega_1$

off-resonant:

$$\Delta\omega_o = \frac{1}{2}\frac{\omega_1^2}{(\omega_o - \omega)}$$

$(\omega - \omega_o)/\omega_1$
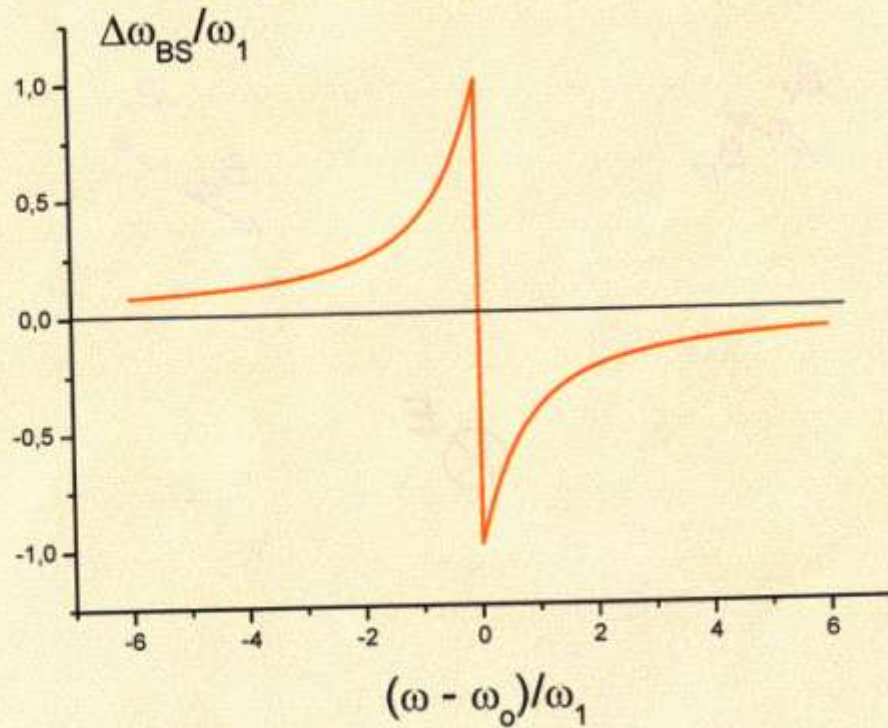
$$\delta\omega_E = -\frac{abv^2}{\omega_o{}^2 - \omega_r{}^2}$$

$$\omega_r = \frac{v}{r}$$

$$\omega_{xy} = ar$$

$$b = \frac{E}{c}\gamma$$

$$= -\frac{abv^2}{\omega_{o^2}} \qquad \omega_o \gg \omega_r$$

$$= abR^2 \qquad \omega_r \gg \omega_o$$

B_o

−v

+v
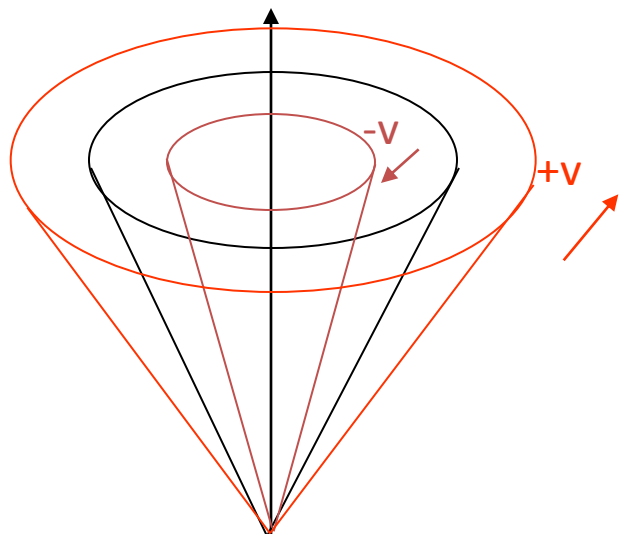
Geometric Phase Picture

Motion of Spins

$$\frac{d\rho}{dt} = -\int_0^t d\tau \left[H_1(t), \left[H_1(t-\tau), \rho(t) \right] \right]$$

$$= \Gamma \rho(t)$$

Or

Bloch equation

$$\frac{d\vec{M}}{dt} = \vec{M} \times \vec{\omega}(t)$$

$$\omega_x(t) = ax + bv_y$$

$$\omega_y(t) = ay - bv_x$$

$$\dot{\theta} = \omega_x(t)\sin\omega_o t - \omega_y(t)\cos\omega_o t$$

$$\theta = \int_0^t dt'\left[\omega_x(t')\sin\omega_o t' - \omega_y(t')\cos\omega_o t'\right]$$
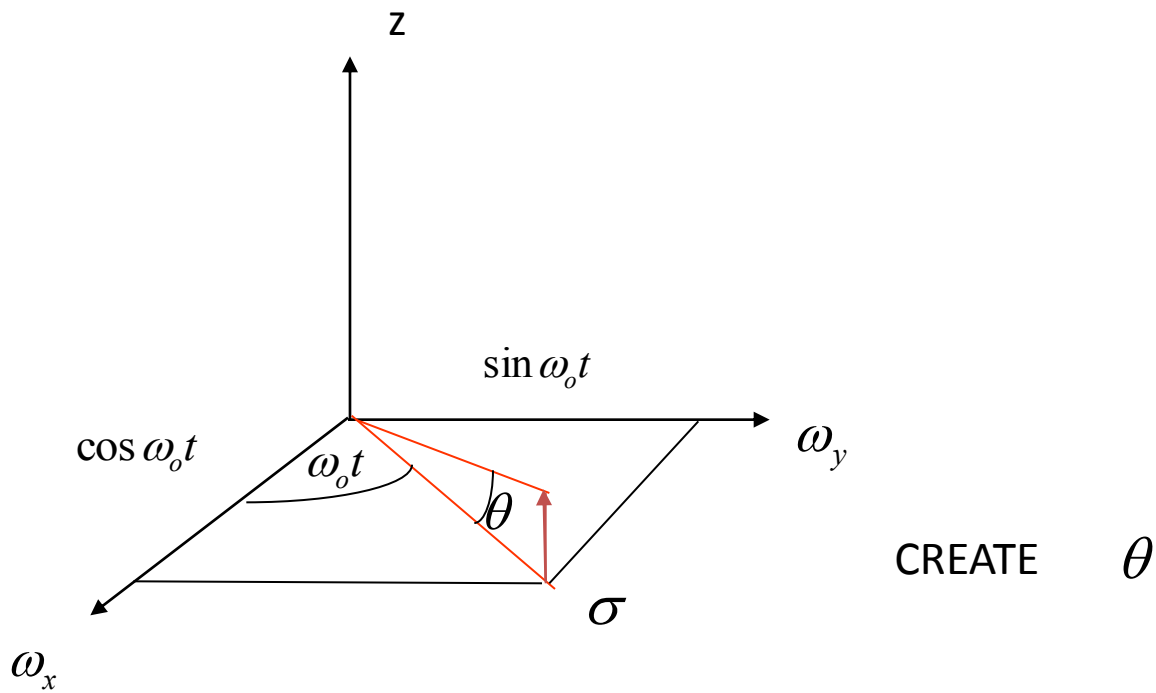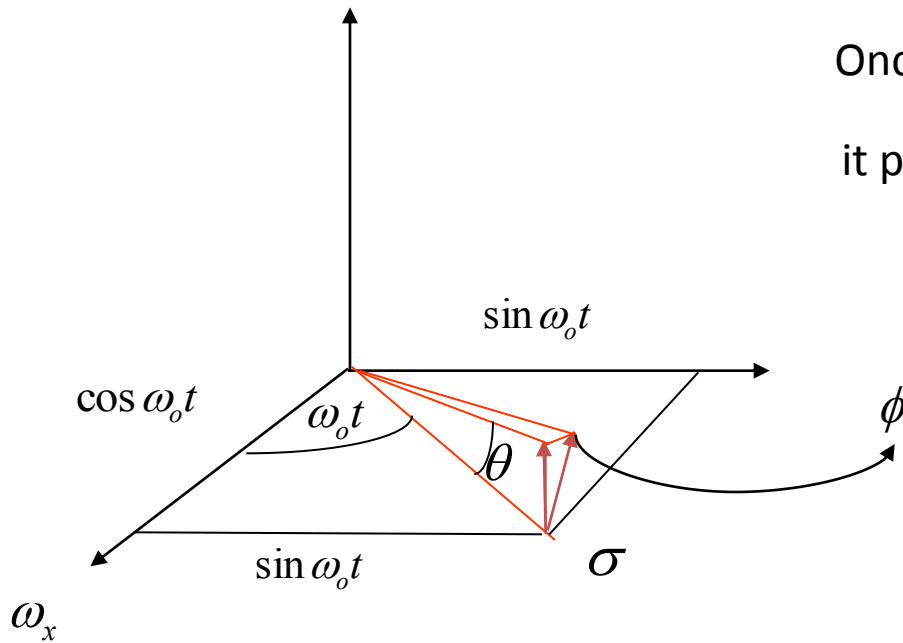
Once θ Builds up

it produces a change in ϕ

$$\dot{\phi} = \theta(t)\left[\omega_x \cos \omega_o t + \omega_y \sin \omega_o t\right]$$

$$\sim \omega_x)t\int dt' \, \omega_y(t')\cos \omega_o t \cos \omega_o t'$$

$$\omega_0 = \gamma B_0', \quad \omega_{x,y}(t) = \gamma B_{x,y}'(t). \qquad (6)$$

The Hamiltonian is thus

$$H = -\frac{\omega_0}{2}\sigma_z - \frac{\omega_x}{2}\sigma_x - \frac{\omega_y}{2}\sigma_y = H_0 + H_1(t). \qquad (7)$$

Defining

$$2b = \omega_x + i\omega_y, \quad 2b^* = \omega_x - i\omega_y, \qquad ($$

the perturbing Hamiltonian can be rewritten as

$$H_1(t) = b^*\sigma_+ + b\sigma_-, \qquad (9)$$

The time evolution of the density matrix is

$$\frac{d\rho}{dt} = -i[H_0 + H_1(t), \rho]. \qquad (11)$$

$$\frac{d\rho}{dt} = -\int_0^t d\tau [H_1(t), [H_1(t-\tau), \rho(t)]] \equiv \Gamma\rho(t), \qquad (18)$$

where Γ is the "relaxation matrix," the real parts of which describe decays of coherence and the imaginary parts of the off-diagonal elements describe frequency shifts.

$$\delta\omega(t) = -\frac{1}{2}\int_0^t \{\cos\omega_0\tau[\omega_x(t)\omega_y(t-\tau) - \omega_x(t-\tau)\omega_y(t)] + \sin\omega_0\tau[\omega_x(t)\omega_x(t-\tau) + \omega_y(t)\omega_y(t-\tau)]\}d\tau.$$

$$(23)$$

Now $\omega_x = ax + bv_y$, $\omega_y = ay - bv_x$ where

$$a = \frac{\gamma}{2} \frac{\partial B_z}{\partial z},$$

$$b = \gamma \frac{E}{c},$$

$$\delta\omega = -\frac{1}{2} \int_0^t d\tau (\cos \omega_0 \tau)\{\langle \omega_x(t)\omega_y(t-\tau)\rangle - \langle \omega_x(t-\tau)\omega_y(t)\rangle\}$$

$$= \frac{ab}{2} \int_0^t d\tau (\cos \omega_0 \tau) R(\tau), \tag{26}$$

where

$$R(\tau) = \langle y(t)v_y(t-\tau) + x(t)v_x(t-\tau) - y(t-\tau)v_y(t)$$

$$- x(t-\tau)v_x(t)\rangle \tag{27}$$

is the net correlation function, where $\langle \cdots \rangle$ represents an ensemble and time average.

$$\delta\omega = \frac{ab}{2} \int_0^t d\tau \cos \omega_o \tau R(\tau)$$

$$R(\tau) = \left\langle \vec{r}(t) \bullet \vec{v}(t-\tau) - \vec{r}(t-\tau) \bullet \vec{v}(t) \right\rangle$$

$$\vec{r}(t) = \int_0^t dt' \, \vec{v}(t')$$

$$R(\tau) = 2h(\tau)$$

$$h(\tau) = \int_0^\tau dt' \left\langle \vec{v}(t) \bullet \vec{v}(t-\tau) \right\rangle = \int_0^\tau dt' \psi(t')$$

Velocity autocorrelation function

$$\delta\omega = -ab \int_{-\infty}^\infty d\omega \frac{\psi(\omega)}{\left(\omega_o^2 - \omega^2\right)}$$

BLOCH SIEGERT

(again)

$$h(\tau) = \int_0^\tau dx \, \psi(x), \qquad \psi(x) = \text{Velocity autocorrelation function}$$

$$\delta\omega = ab \left[\int_0^t d\tau \cos \omega_0 \tau \int_{-\infty}^\infty \psi(\omega) \frac{\sin \omega \tau}{\omega} d\omega \right], \qquad \delta\omega = -ab \int_{-\infty}^\infty \frac{\psi(\omega)}{(\omega_0^2 - \omega^2)} d\omega.$$

Bloch-Siegert again

EXAMPLE

Circular orbit

$$\psi(\tau) = v^2_{xy} \cos \omega_r \tau$$
$$\psi(\omega) = v^2_{xy} \delta(\omega - \omega_r)$$

$$\delta\omega = \frac{abv^2_{xy}}{\omega_o^2 - \omega_r^2}$$

Bloch Siegert
result

Short correlation times $\implies$ high frequencies

$$\psi(\tau) = \langle v^2 \rangle e^{-\tau/\tau_c}$$

$$\delta\omega = -\frac{ab\langle v^2 \rangle}{\omega_o^2} \frac{1}{[1 + 1/\omega_o \tau_c]}$$

Long correlation times $\implies$ low frequencies

Diffusion limit......bounded diffusion

$$G(r,t) \implies S(q.\omega)$$

$$\psi(\omega) = \lim_{q \to 0} 2 \frac{\omega^2}{q^2} S(q,\omega) \qquad \text{Egelstaff, de Gennes}$$

Physical content

$$\psi(\tau) = \frac{\partial^2}{\partial \tau^2} \left\langle \vec{r}(t) \bullet \vec{r}(t-\tau) \right\rangle$$
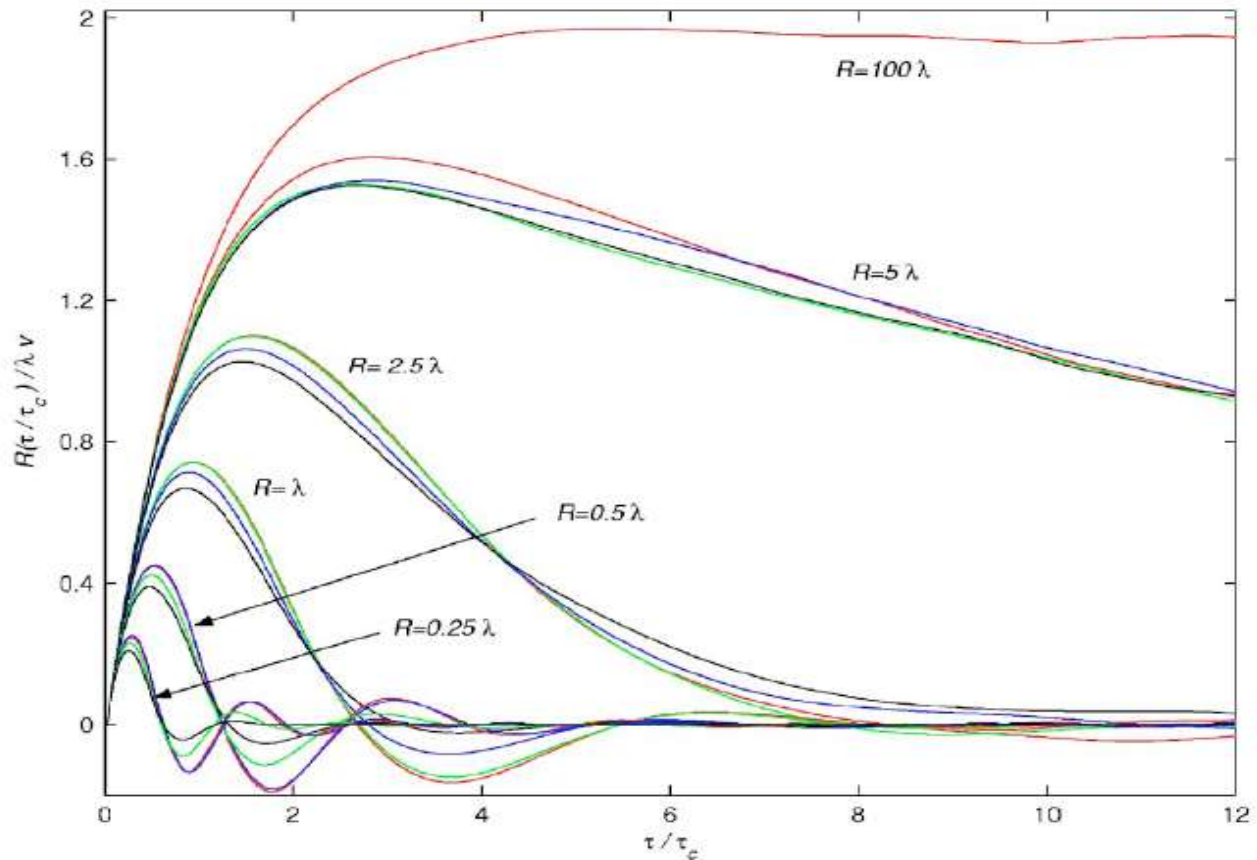
FIG. 1. The position-velocity correlation function $R(\tau)=2h(\tau)$ as a function of cell radius R parametrized in terms of the mean free path λ for different degrees of specularity as parametrized by the angular spread of the final angle compared to the incident angle. The plots for a given R are for angular spreads on reflection of $0°$, $45°$, $90°$, and $180°$, with the latter representing diffuse reflection. Increased angular spread causes the correlation function to decay more rapidly in all cases. For $R \gtrsim 2.5\lambda$, there was practically no effect due to the degree of specularity, as expected.
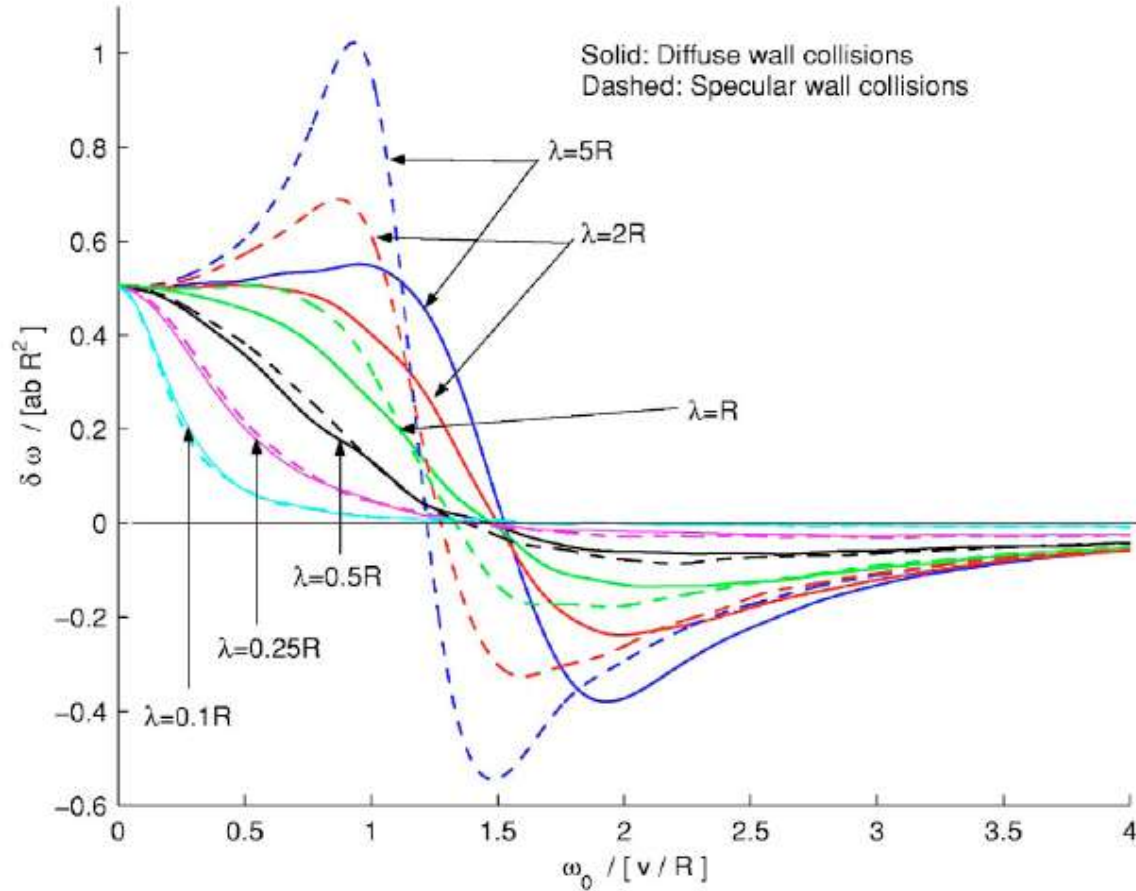
FIG. 3. Results of numerically applying Eq. (37) to numerical calculations of the correlation function, for varying λ with R fixed
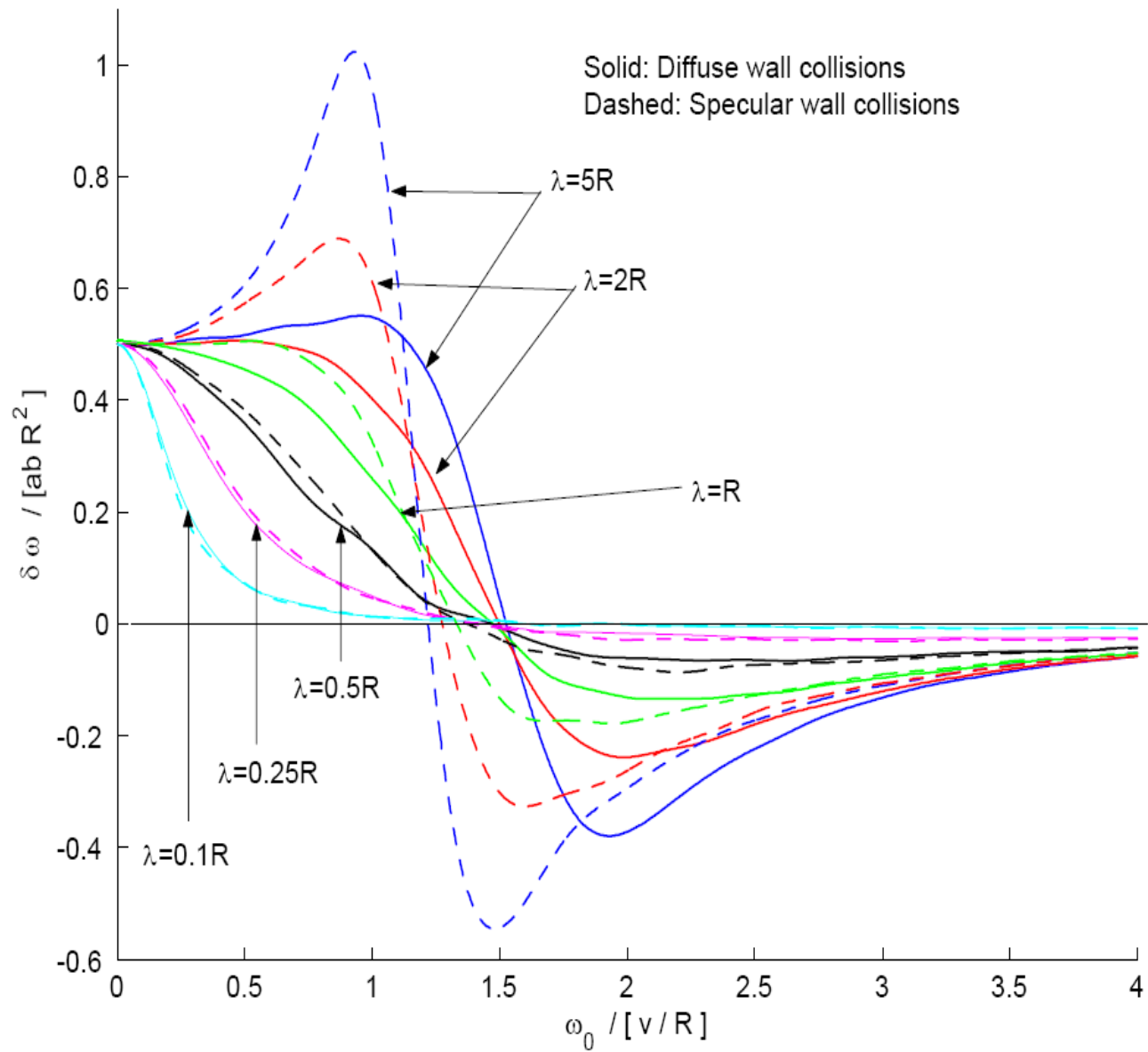
Figure 1: Note the curves are for a single fixed velocity. The velocity dependence is contained in the normalization of the frequency scale, $\omega_r = v/R$.

Linear electric field frequency shift (important for next generation electric dipole moment searches) induced in confined gases by a magnetic field gradient.

A.L. Barabanov[#], R. Golub[+] and S.K. Lamoreaux[*]

$$\delta\omega = \frac{ab}{2}\lim_{\tau\to\infty}\int_0^{\tau} R(t)\cos(\omega_0 t)dt, \qquad R(\tau) = \langle \vec{r_\perp}(t)\cdot\vec{v_\perp}(t-\tau) - \vec{r_\perp}(t-\tau)\cdot\vec{v_\perp}(t)\rangle.$$

According to [11] the correlation function $R(\tau)$ is determined by the velocity autocorrelation function,

$$\psi(t) \equiv \langle \vec{v}_\perp(t)\cdot\vec{v}_\perp(0)\rangle,$$

namely,

$$R(\tau) = 2\int_0^{\tau} \psi(t)dt.$$
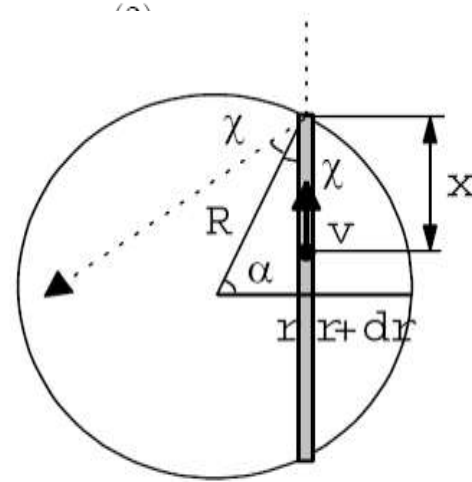
Figure 2: Trajectory of a particle in a cylindrical cell.

As a result, for the time $l \cdot \tau_w < t < (l+1) \cdot \tau_w$ $(l = 0, 1, 2 \ldots)$ the function f is given by

$$f(x, \alpha, t) = \begin{cases} \cos(2(l+1)\alpha), & 0 < x < v(t - l \cdot \tau_w), \\ \cos(2l\alpha), & v(t - l \cdot \tau_w) < x < 2R\sin\alpha, \end{cases} \quad (14)$$

Then performing the averaging (13) the autocorrelation function takes the form:

$$\psi(\alpha, t) = v^2 \left(A_l + B_l \frac{t}{\tau_w} \right), \quad (15)$$

where

$$A_l = (l+1)\cos(2l\alpha) - l\cos(2(l+1)\alpha), \quad (16)$$

$$B_l = \cos(2(l+1)\alpha) - \cos(2l\alpha). \quad (17)$$

Spectrum of the velocity correlation function

$$-\Delta\omega(\alpha) = ab \int_{-\infty}^{\infty} \frac{\Psi(\alpha, \omega)}{(\omega_o^2 - \omega^2)} d\omega$$

we find

$$-\Delta\omega(\alpha) = \left(\frac{v}{\omega_o} \right)^2 ab \left(1 + \frac{\sin^2\alpha \sin 2\delta_o}{2\delta_o \sin(\delta_o - \alpha) \sin(\delta_o + \alpha)} \right) \quad (26)$$

This formula was originally derived in [10], (equ. 78) by direct solution of the classical Bloch equations and the result shows the equivalence of the two methods.

2.2.3 Combined influence of gas and specular wall collisions

The velocity autocorrelation function in the absence of collisions is given by the sum of the motions of a group of harmonic oscillators (28). In the presence of gas collisions the individual oscillators $\psi_n^{\pm}(\alpha, t)$ will obey the equation for a damped harmonic oscillator which is the combination of (31) and (29), i.e.

$$\frac{d^2\psi_n(t)}{dt^2} + \frac{1}{\tau_c}\frac{d\psi_n(t)}{dt} + \omega_n^2\psi(t) = 0, \qquad (32)$$

with the initial condition:

$$\psi_n^{\pm}(\alpha, 0) = v^2. \qquad (33)$$

$$-\Delta\omega\left(\alpha\right) = R^2 ab \sin^2\alpha \sum_{m=-\infty}^{\infty} \frac{1}{\left(\alpha + \pi m\right)^2} \left[\frac{\left(\omega_o'^2 - \frac{(\alpha + \pi m)^2}{\sin^2\alpha}\right)}{\left(\left(\omega_o'^2 - \frac{(\alpha + \pi m)^2}{\sin^2\alpha}\right)^2 + \omega_o'^2 r_o^2\right)} \right]$$

(42)

that is we go from the collision free case to the case of gas collisions by replacing

$$f_\alpha\left(\omega'\right) = \frac{1}{\left(\omega_o'^2 - \frac{(\alpha + \pi m)^2}{\sin^2\alpha}\right)}$$

in (25) by the square bracket in (42) or by replacing $f_\alpha\left(\omega'\right)$ by $f_\alpha\left(\omega'\sqrt{1 + i\frac{r_o}{\omega'}}\right)$ and taking the real part. Since we have evaluated the summation (25) we obtain the frequency shift by making the equivalent transformation to (26)

$$-\Delta\omega\left(\alpha\right) = R^2 ab \sin^2\alpha \, \mathrm{Re}\left\{ F_P(\alpha, \delta = \delta_o\sqrt{1 + \frac{i}{\omega_o \tau_c}}) \right\}$$

(43)

where

$$F_P(\alpha, \delta) = \left(1 + \frac{\sin^2\alpha \sin 2\delta}{2\delta \sin\left(\delta - \alpha\right)\sin\left(\delta + \alpha\right)}\right)\frac{1}{\delta^2}$$

(remember $\delta_o = \omega_o \tau_w/2$). For a fixed velocity we average over α, according to (10):

$$\Delta\omega = \int_0^{\pi/2} d\alpha P\left(\alpha\right) \Delta\omega\left(\alpha\right)$$

(44)
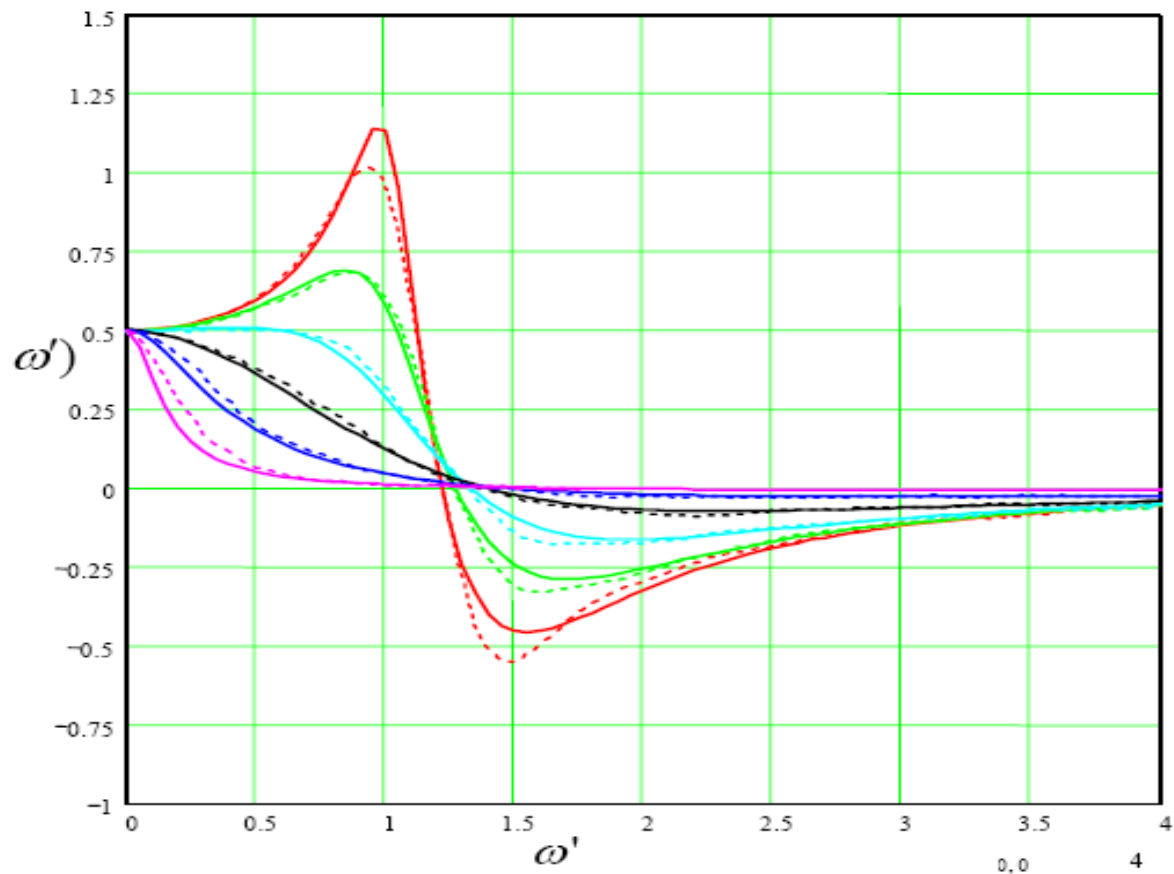
Figure 3: Normalized frequency shift for a constant velocity as a function of normalized applied frequency, $\omega' = \omega_o R/v$, for different values of the damping parameter $r_o = R/\lambda$. Solid curves - results of the analytic function, equations (43) and (44). Dotted lines numerical simulations from ref. [11]. red - $r_o = .2$, green - $r_o = .5$, cyan - $r_o = 1$, black $r_o = 2$, blue - $r_o = 4$, magenta - $r_o = 10$.
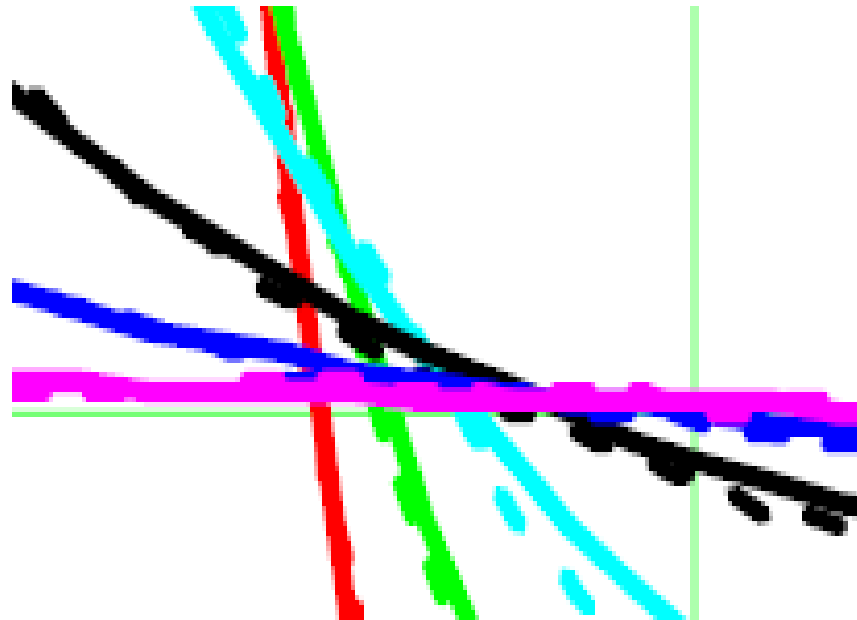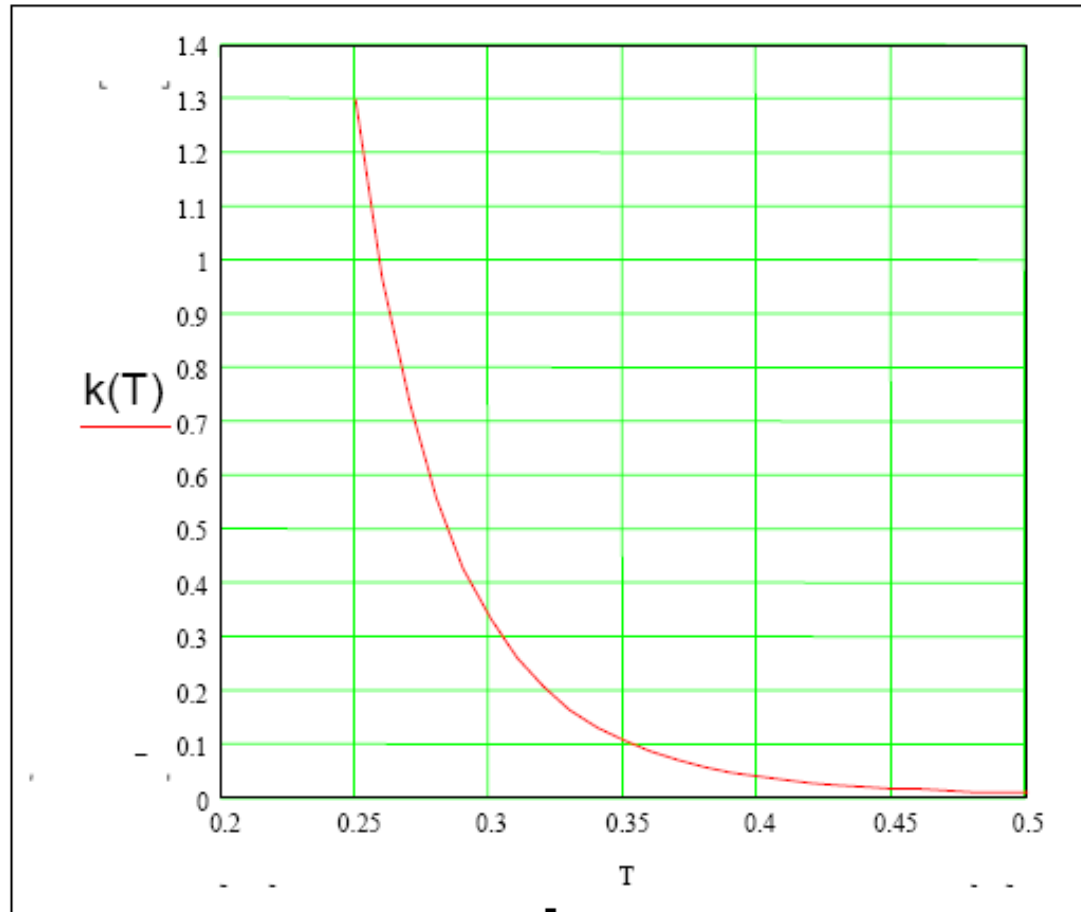
Figure 3. Dependence of $k = \lambda(T)/R$ on temperature

He^3
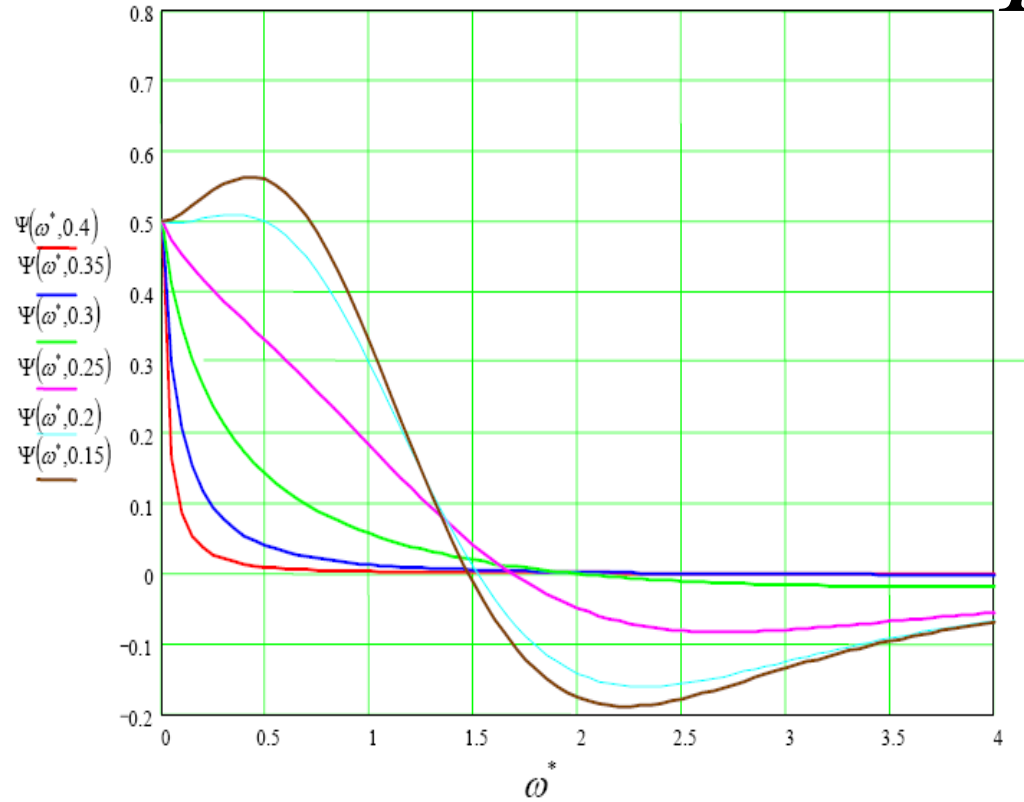
Figure 4: Normalized velocity averaged frequency shift vs. reduced frequency $\omega^*=\omega_o R/\beta\left(T\right)$ for various temperatures using the temperature-dependent mean free path for He^3 in He^4.
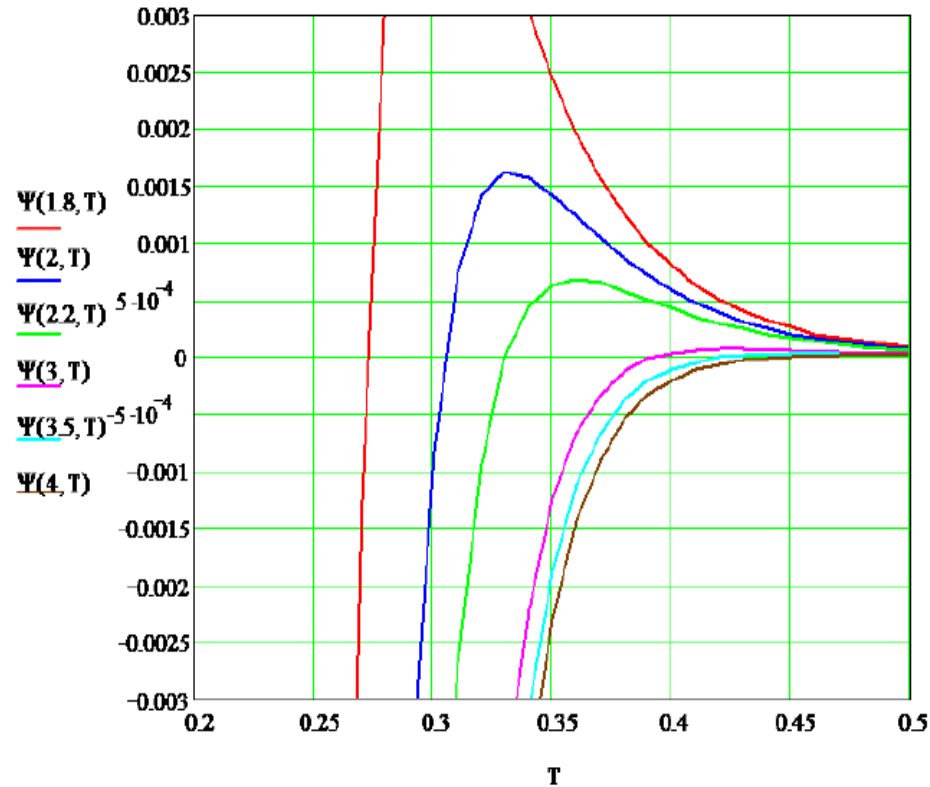
Figure 5: Normalized velocity-averaged frequency shift, $\Psi\left(\omega^{*}, T\right)$ vs. temperature, T, for various reduced frequencies $\omega^{*}=\omega_{o} R / \beta\left(T\right)$ using the temperature-dependent mean free path for He^{3} in He^{4}

where we recognize that the correlation function $R_{\vec{r}\,\vec{r}}\,(\tau)$ is an even function of τ. A measurement of T_1 will thus yield the function $S_r\,(\omega)$. Now

$$\omega^2 S_r\,(\omega) = -\int_{-\infty}^{\infty} R_{\vec{r}\,\vec{r}}\,(\tau)\,\frac{d^2}{d\tau^2}\,(\cos\omega\tau)\,d\tau$$

$$= -\int_{-\infty}^{\infty} \frac{d^2 R_{\vec{r}\,\vec{r}}\,(\tau)}{d\tau^2}\,(\cos\omega\tau)\,d\tau$$

$$= \int_{-\infty}^{\infty} R_{\vec{v}\,\vec{v}}\,(\tau)\,(\cos\omega\tau)\,d\tau$$

where we used $R_{\vec{v}\,\vec{v}}\,(\tau) = -d^2 R_{\vec{r}\,\vec{r}}\,(\tau)\,/d\tau^2$ [16] for the velocity correlation function. Then

$$R_{\vec{v}\,\vec{v}}\,(\tau) = \frac{1}{2\pi}\int_{-\infty}^{\infty} \omega^2 S_r\,(\omega)\cos\omega\tau d\tau$$